1 **Role of atmospheric aerosols in severe winter fog over Indo Gangetic Plains of India: a**

2 **case study**

3 Chandrakala Bharali[1], Mary Barth[2], Rajesh Kumar[2], Sachin D. Ghude[3], Vinayak Sinha[4], Baerbel Sinha[4]

4 [1] Department of Physics, Dibrugarh University, Dibrugarh, Assam, India

5 [2] NSF National Centre for Atmospheric Research, Boulder, CO, US

6 [3] Indian Institute of Tropical Meteorology, Ministry of Earth Sciences, Pune, India

7 [4] Department of Earth and Environmental Sciences, Indian Institute of Science Education and Research, Mohali,

8 Punjab, India

9 **Correspondence:** chandrakalabharali@gmail.com, barthm@ucar.edu

11 **Abstract**

12 Winter fog and severe aerosol loading in the boundary layer over North India, particularly in the Indo-

13 Gangetic Plain (IGP), disrupt daily life of millions of people in the region. To understand better the

14 role of aerosol-radiation feedback on the occurrence, spatial extent, and persistence of winter fog; and

15 the associated aqueous chemistry in fog in the IGP, several model simulations have been performed

16 using the Weather Research and Forecasting model coupled with chemistry (WRF-Chem). While

17 WRF-Chem was able to represent the fog formation for the December 23-24, 2017 fog event over the

18 central IGP in comparison to station and satellite observations, the model underestimated $PM_{2.5}$

19 concentrations compared to the Central Pollution Control Board of India monitoring network. While

20 evaluating aerosol composition for fog events in IGP, we found that the WRF-Chem aerosol

21 composition was quite different from measurements obtained during the Winter Fog Experiment in

22 Delhi, with secondary aerosols, particularly chloride aerosol fraction being strongly underpredicted

23 (~66.6%). Missing emission sources (e.g., industry and residential burning of cow dung and trash) and

24 aerosol and chemistry processes need to be investigated to improve model-observation agreement. By

25 investigating a fog event on December 23-24, 2017 over central IGP, we found that the aerosol-

26 radiation feedback weakens turbulence, lowers the boundary layer height, and increases $PM_{2.5}$

27 concentrations and RH within the boundary layer. Factors affecting the feedback include loss of

28 aerosols through deposition of cloud droplets and internal mixing of absorbing and scattering aerosols.

29 Aqueous-phase chemistry increases the $PM_{2.5}$ concentrations, which subsequently affects the aerosol-

30 radiation feedback by both increased mass concentrations and aerosol sizes. With aerosol-radiation

31 interaction and aqueous phase chemistry, fog formation began 1-2 hours earlier and caused a longer

32 fog duration than when these processes were not included in the WRF-Chem simulation. The increase

33 in RH in both the experiments is found to be important for fog formation as it promoted the growth of

34 aerosol size through water uptake, increasing the fog water content over IGP. The results from this

study suggest that the aerosol-radiation feedback and secondary aerosol formation play an important role in the air quality and the intensity and lifetime of fog over IGP, yet other feedbacks, such as aerosol-cloud interactions, need to be quantified.

1   Introduction

The Indo-Gangetic Plain (IGP; 21°35′-32°28′N latitude. and 73°50′-89°49′E longitude) in the northern part of the Indian subcontinent is one of the most densely populated and heavily polluted regions in South Asia. The rapid population and economic growth in the IGP region over the last decade have increased air pollution over this region. This is evident from the increasing trend in AOD and NO_2 column concentration over India reported in recent studies (Dey and Di Girolamo, 2011; Ghude et al., 2013; Krishna Moorthy et al., 2013), which has slowed and reversed only recently (Sarkar et al., 2019). The high concentration of aerosols along the IGP and their adverse effects on human health and the environment are increasing (Ghude et al., 2016). Consequently, more than 500 million people living in the IGP breathe air that exceeds the National Ambient Air Quality Standards (NAAQS), which has reduced the life expectancy of the people (Debnath et al., 2022; Lelieveld et al., 2015). Lelieveld et al., (2015) estimated a very high number of premature deaths (0.716 million per year) linked to aerosols ($PM_{2.5}$), thus making Southeast Asia one of the largest regions affected by premature mortality globally.

One of the major environmental concerns in the IGP is the urban air quality during winter, especially over the mega-cities, e.g., Delhi, located in the north-western part of IGP (Ghude et al., 2020; Jena et al., 2021; Sengupta et al., 2022). Several urban air pollution hotspots along the IGP extend from northwest to east with monthly average $PM_{2.5}$ greater than 200 μgm^{-3} (NAAQS=60μgm^{-3}, 24 hr average) in the winter season (Bharali et al., 2019; Krishna et al., 2019). IGP is dominated mainly by fine mode particulates, especially over central to eastern IGP, during post-monsoon and winter (Kumar et al., 2018). Biomass burning (agricultural waste burning, domestic heating, etc.) is an important contributor to the observed high $PM_{2.5}$ loading over IGP during these seasons (Kulkarni et al., 2020; Pant et al., 2015; Pawar and Sinha, 2022; Sharma et al., 2010; Yadav et al., 2020). Delhi is affected substantially by the emissions from agricultural waste burning in the north-western states of Punjab and Haryana during the post-monsoon (October-November) season (Badarinath et al., 2009; Jethva et al., 2018; Kumar et al., 2021). Studies showed that $PM_{2.5}$ increased from ~50 $\mu g\ m^{-3}$ to as high as 300 $\mu g\ m^{-3}$ (Ojha et al., 2020), and AOD reached 0.98 with the presence of absorbing aerosols (Singh et al., 2018) during the peak biomass burning in post-monsoon.

IGP experiences fog (both radiation and advection fog) every winter after the passage of the synoptic wind system called the "Western Disturbances". The majority of fog events in the IGP during December-January are radiation fog (Deshpande et al., 2023; Ghude et al., 2023), formed due to radiative cooling of the surface. The number of low visibility days due to haze/fog formation has been

71 increasing significantly (Ghude et al., 2017; Jenamani, 2007; Singh and Dey, 2012), impacting socio-
72 economic activities, e.g., aviation (Kulkarni et al., 2019). The increase in the intensity and regional
73 extent of fog over IGP is consistent with the increasing trend in aerosol concentration due to
74 increasing anthropogenic emissions (Sarkar et al., 2006; Syed et al., 2012).

75   Several factors control the formation and persistence of fog in the IGP, e.g., stable boundary
76 layer, low temperature, availability of moisture (supplied by the Western Disturbances and irrigation
77 activities), and the aerosol number and composition (Acharja et al., 2022; Dhangar et al., 2021). It has
78 also been suggested that the atmospheric rivers (moisture incursion from Arabian Sea) act as a source
79 of water vapor over IGP, which fuels the intensification of fog and haze (Verma et al., 2022) during
80 winter. The high aerosol concentration in the boundary layer influences fog formation (Gautam et al.,
81 2007; Safai et al., 2019) over the IGP by providing the needed cloud condensation nuclei (CCN) for
82 activation into fog droplets. In addition, aerosols induce surface cooling by reducing solar radiation at
83 the surface while warming the lower troposphere by absorption (Ding et al., 2016; Yu et al., 2002). A
84 reduction in surface-reaching solar radiation by ~19% has been reported during winter over Kanpur in
85 the IGP (Dey and Tripathi, 2007). The reduced solar flux affects the boundary layer stability and
86 depth by suppressing the thermals and thus further increasing the surface aerosol concentration via
87 aerosol-radiation feedback, which is very strong over the IGP (Bharali et al., 2019). Kumar et al.,
88 (2020) have shown that aerosol-radiation feedback significantly improves the accuracy of $PM_{2.5}$ and
89 temperature forecasts in Delhi. Srivastava et al., (2018) reported that the direct aerosol forcing over
90 polluted regions is very large with values up to -80.0 ± 7.2 W m^{-2} over the IGP in the winter season.

91   Aerosol-radiation interaction determines that the aerosol distribution is critical for the evolution
92 of fog (Bodaballa et al., 2022; Steeneveld et al., 2015), while microphysics is important for fog
93 formation and dispersal (Boutle et al., 2018; Maalick et al., 2016). Although the relationship between
94 the aerosol chemical composition and aerosol activation to CCN has not been fully understood yet,
95 studies have found that the chemical composition and mixing state of aerosols affect the
96 hygroscopicity (κ) of aerosols (Bodaballa et al., 2022; Ma et al., 2013; Moore et al., 2012; Zhang et
97 al., 2014a). Fog processes involve a complex interplay between local meteorology, radiation,
98 microphysics, and aerosol chemistry, making it difficult to understand the fog lifecycle (Acharja et al.,
99 2022; Maalick et al., 2016; Zhang et al., 2014b). There is considerable heterogeneity in the spatial and
100 temporal aerosol properties over IGP and the poor estimates of their mixing state. Therefore,
101 prediction of fog by weather models is still challenging with biases in fog's onset and dispersal
102 timings.

103   Previous studies have focussed on the impacts of meteorological conditions, topography, or
104 anthropogenic emissions on the poor air quality and intensification of fog during winter over IGP (e.g.
105 Hakkim et al., 2019). However, studies on the effect of feedback induced by the aerosols on the
106 meteorological conditions and thus on aerosol concentration are very limited over this region, except
107 for a few above-mentioned studies which discuss how the aerosol-radiation feedback favors haze and

108 fog during winter. Moreover, fog can provide a medium for aqueous-phase reactions. While several
109 earlier studies have reported an increase in secondary aerosols during fog over IGP, a sensitivity study
110 examining the impact of fog on aqueous phase chemistry has not yet been done over IGP.

111   In the present work, we aim to find the suitable chemistry/physics as well as the meteorology
112 initial/boundary conditions that lead to improved simulations of fog events in the Weather Research
113 and Forecasting model coupled with chemistry (WRF-Chem; (Fast et al., 2006; Grell et al., 2005;
114 Powers et al., 2017). We also explore the role of aerosol-radiation feedback on fog properties as the
115 high aerosol loadings in northern India can impact the heating rates, temperature inversions, and
116 boundary layer height. The role of aqueous chemistry on fog properties and vice-versa is also
117 investigated.

118

119   **2   Methodology**

120 Fog formed due to radiative cooling, based on the onset time of fog and low wind speeds (Deshpande
121 et al., 2023 and references therein), at the surface on both 23rd and 24th December 2017 over a
122 widespread region of the IGP (Fig. 1a, b). The fog region is located over an area with high $PM_{2.5}$
123 anthropogenic emissions (Fig. 1c). The IGP is a large region with varying meteorology and aerosol
124 characteristics, therefore, it is divided into three areas, northwest (NWIGP: latitude-longitude range,
125 27°N-32°N,75°E-79°N), central (CIGP: latitude-longitude range, 25°N-28°N,79°E-83°E), and east
126 (EIGP: latitude-longitude range, 24°N-27°N, 83°E-87°E) which are marked by the black rectangles in
127 Fig.1c. Although biomass burning and anthropogenic emissions dominate throughout the IGP during
128 post-monsoon and winter season, the north-westerly wind system results in the gradient distribution of
129 AOD over this region. The downwind regions, CIGP and EIGP are influenced by the long-range
130 transport from the NWIGP, resulting in high AOD with dominant fine particulates over CIGP and
131 EIGP, especially during post-monsoon and winter (Kedia et al., 2014; Kumar et al., 2018). Therefore,
132 representative stations from each region listed in section 2.2 are considered for the sensitivity
133 analyses.

134

135 **2.1 Modeling**

136   The WRF-Chem model version 4.0.3 is used for this study. Earlier studies have successfully
137 used WRF-Chem to predict fog (Pithani et al., 2019) and in the study of aerosol-radiation feedback on
138 air quality (Kumar et al., 2020; Bharali et al., 2019) and fog (Shao et al., 2023). The model domain is
139 centered at Delhi (77.1°E, 28.7°N) with 300 grid points in the east-west, 170 grid points in the south-
140 north direction (Fig. 1c), and 50 vertical eta levels with the model top at 50 hPa. The horizontal grid
141 spacing of the domain is 10 km, while the vertical grid spacing varies from higher resolution (~200 m)
142 in the boundary layer to coarser resolution (~1200 m) near the model top. We conduct three model
143 configurations (Table 1) for December 20-24, 2017 to identify the best configuration for
144 meteorological simulations. The three experiments have been designed with different combinations of

meteorological initial/lateral boundary conditions and planetary boundary layer (PBL) physics. Experiment 1 (EXP1) uses the National Centers for Environmental Predictions (NCEP) Final Analysis (GFS-FNL; 1° x1°, 6 hourly) meteorology data for initial and boundary conditions and the YSU (Yonsei University; (Hong et al., 2006) PBL scheme. Experiments 2 and 3 (EXP2, EXP3) use ERA-Interim Project (1.125° x 0.703°, 6 hourly) for meteorology initial and boundary conditions. EXP2 uses the YSU PBL scheme while EXP3 uses the ACM2 (Asymmetric Convective Model version 2) PBL scheme. ACM2, is a hybrid of the original nonlocal closure (Pleim and Chang, 1992) and a local closure eddy diffusion scheme (Pleim, 2007a, 2007b). The YSU PBL option was coupled with the Noah LSM while ACM2 was coupled with Pleim-Xiu LSM. While YSU permits investigations of both aerosol-radiation (AR) and aerosol-cloud interactions (ACI), ACI is not possible when using the ACM2 PBL scheme because in WRF the ACM2 PBL scheme does not provide the exchange coefficient for heat, which is required to calculate the maximum supersaturations and therefore the activation fraction for aerosol mass and number for each bin/mode, which is based on the Abdul-Razzak and Ghan, (2002) scheme. However, ACM2 has been shown to perform well for air quality in the polluted regions (Mohan and Gupta, 2018; Gunwani and Mohan, 2017; Xie et al., 2012, Mohan and Bhati, 2011). Mohan and Gupta (2018) tested the YSU and ACM2 schemes during the summer time (1-15 June 2010) and focused on the evaluation of temperature, wind speed, PBL height, ozone, and PM_{10}. Although these studies recommend using the nonlocal ACM2 PBL scheme for air quality prediction for IGP, there are still seasonal, day-night, and regional biases in the PBL schemes. Gunwani and Mohan (2017) showed that ACM2, QNSE (Quasi Normal Scale Elimination), and MYJ (Mellor-Yamada-Janjić) schemes work well in predicting temperature, humidity, and wind speed in different regions of India. Mohan and Bhati (2011) found that using the ACM2 PBL scheme with Pleim Xiu surface physics improved wintertime meteorology estimates in Delhi indicating its potential in fog predictions, whereas Pithani et al., (2019) recommend using the local PBL scheme MYNN2.5 (Mellor-Yamada-Nakanishi-Niino level 2.5). Shin and Hong (2011) found that a non-local (e.g., ACM2, YSU) scheme is favorable in unstable conditions and a local scheme (e.g., MYJ, Boulac) in stable conditions. All these studies suggest the need for careful consideration of the above-mentioned biases while selecting a PBL scheme. Therefore, to ensure that WRF captures all the relevant meteorological parameters including relative humidity reasonably well during fog events in winter, we designed EXP1, EXP2 and EXP3.

The advantage of Pleim-Xiu LSM (PX-LSM) is that it allows nudging of soil moisture and temperature to improve the prediction of meteorology near the surface (Pleim and Gilliam, 2009; Pleim and Xiu, 2003; Xiu and Pleim, 2001) which Noah LSM does not include. The PX-LSM includes two-layer soil (0–1 and 1–100 cm) model, canopy moisture, and aerodynamic and stomatal resistance. Ground surface (1 cm) temperature is calculated from the surface energy balance using a force-restore algorithm for heat exchange within the soil. Although the two-layer approach in PX-LSM is less detailed than the multilayer soil models such as the Noah LSM (four soil layers; Chen and

182 Dudhia 2001), it performs well with realistic initialization for soil moisture and through dynamic
183 adjustment in the model simulation where soil moisture is indirectly nudged according to differences
184 in 2-m temperature (T2) and 2-m relative humidity (RH) between the model and observation (Pleim
185 and Xiu, 2003).Soil moisture nudging adjusts the surface evaporation (direct soil surface evaporation,
186 vegetative evapotranspiration, and evaporation from wet canopies) which then affects the partitioning
187 of available surface energy into latent and sensible heat flux and thus reduces errors in T2 and 2-m
188 RH.

189 For EXP2, meteorological initial conditions were refreshed every 24 hours, while EXP3 was a
190 continuous run but soil moisture was nudged to the Era-Interim dataset to improve the prediction of
191 surface fluxes. All other physics and chemistry options are the same for all the experiments except the
192 surface physics option, which changes with the PBL scheme used. The deposition of cloud droplets is
193 an important moisture and aerosol sink during fog events. For all these simulations, the deposition
194 velocity of cloud droplets was reduced to 0.01 m s^{-1} based on Stoke's Law and previous studies
195 (Katata et al., 2015; Tav et al., 2018) because its default value (0.1 m s^{-1}), is large.

196 To examine the radiative effects of aerosols and aqueous phase chemistry additional
197 simulations have been done using the meteorological configuration in EXP3, with aerosol-radiation
198 (wFB) feedback plus aqueous chemistry (wAq.chem), without aerosol-radiation feedback (nFB) but
199 with aqueous chemistry, and without aqueous chemistry (noAq.chem) but with aerosol-radiation
200 feedback. The analysis has been done for the fog events on 23rd and 24th December 2017 as

201

202 $$F_{ARF}=P(wFB-nFB)$$

203 $$F_{Aq.chem}= P (wAq.chem-noAq.chem)$$

204 where F_{ARF} is the impact due to aerosol radiation feedback on the meteorological parameters/chemical
205 species (P) and $F_{Aq.chem}$ is the impact due to the inclusion of aqueous phase chemistry

206

207 Emissions used in the WRF-Chem simulations are from the EDGAR-*HTAP v2 (Emissions*
208 *Database for Global Atmospheric Research- Hemispheric Transport of Air Pollution;0.1° x 0.1°)*
209 inventory for anthropogenic emissions and *FINN v*2.2 *(Fire INventory from NCAR; 1 km x 1 km) fire*
210 emission inventory (Wiedinmyer et al., 2011). Trash-burning emissions (Chaudhary et al., 2021) are
211 also included in the simulations. The model calculates the biogenic emissions online using MEGAN
212 v2.04 (*Model of Emissions of Gases and Aerosols from Nature*) (Guenther et al., 2006). The initial and
213 lateral boundary conditions for chemical constituents are from the global chemistry transport model
214 CAM-Chem (*Community Atmosphere Model with Chemistry*) (Emmons et al., 2020).

215 The MOZART (Model for Ozone and Related chemical Tracers) chemical mechanism
216 (Emmons et al., 2010) is used for gas-phase chemistry, which includes 85 gas-phase species, 39
217 photolysis, and 157 gas-phase reactions. It has been updated to include an explicit treatment of
218 aromatic compounds, HONO, C_2H_2, and isoprene oxidation scheme (Knote et al., 2014). The lumped

toluene used by Emmons et al., (2010) has been speciated into benzene, toluene, and lumped isomers of xylenes (Knote et al., 2014). For this study, HCl emissions, transport, dry, and wet deposition are represented. However, HCl gas-phase reaction is not included in MOZART.

The Model for Simulating Aerosol Interactions and Chemistry (MOSAIC) with four size bins (0.039–0.156, 0.156–0.625, 0.625–2.500, and 2.5–10.0 µm dry diameters) coupled with MOZART gas-phase chemistry is used (Fast et al., 2006; Zaveri et al., 2008). The bin sizes are defined by their lower and upper dry particle diameters, so there is no transfer of particles between bins during water uptake or loss. It is assumed that aerosols in each bin are internally mixed with the same chemical composition while they are externally mixed in different bins.

The aerosol composition includes sulfate (SO_4^{2-}), ammonium (NH_4^-), nitrate (NO_3^-), aerosol water, sea salt (Na^+, Cl^-), methanesulfonate (CH_3SO_3), carbonate (CO_3^{2-}), calcium (Ca^+), black carbon (BC), organic mass (OC), and unspecified inorganic species such as silica, inert minerals, and trace metals lumped together as other inorganic mass (OIN). For OC, primary OC and secondary OC are represented separately, where the latter is simulated using the volatility basis set (VBS) approach. Reactive inorganic species such as potassium (K^+) and magnesium (Mg^+) are usually present in much smaller amounts and are equivalent to Na^+ since their sulfate, nitrate, and chloride salts are similar in terms of their solubility in water.

MOSAIC treats condensation and evaporation of trace gases to/from particles, nucleation (new particle formation), and coagulation. Aerosol coagulation (Brownian) is based on (Jacobson et al., 1994) and nucleation is based on (Wexler et al., 1994) parameterization of H_2SO_4-H_2O homogeneous nucleation. Sulfate, nitrate, chloride, and ammonium aerosols are mainly formed through oxidation and neutralization/condensation of gas precursors. Gas-phase sulfuric acid (H_2SO_4) is produced by the gas-phase oxidation of SO_2 by OH and nitric acid (HNO_3) formation is via the oxidation of NO_2 by OH. HCl is a primary emission product. The neutralization/condensation of H_2SO_4, HCl, and HNO_3 with NH_3 produces ammonium such as ammonium sulfate ((NH_4)$_2SO_4$), ammonium bisulfate (NH_4HSO_4), ammonium chloride (NH_4Cl) and ammonium nitrate (NH_4NO_3), respectively. The thermodynamic modules in MOSAIC for the dynamic gas-particle partitioning of aerosols MTEM (Multicomponent Taylor Expansion Method) and MESA (Multicomponent Equilibrium Solver for Aerosols) calculate the activity coefficient in aqueous phase aerosols and compute the intraparticle solid-liquid phase equilibrium respectively (Zaveri et al., 2005, 2008). The Adaptive Step Time-split Euler Method (ASTEM) coupled with MESA-MTEM dynamically integrates the mass transfer equations.

Aqueous-phase chemistry uses a bulk water approach employing the Fahey and Pandis (2001) mechanism. It calculates sulfate formation, formaldehyde oxidation, and non-reactive uptake of nitric acid, hydrochloric acid, ammonia, and other trace gases (Chapman et al., 2009; Pye et al., 2020). Aqueous-phase sulfate is produced via oxidation of SO_2 by H_2O_2, O_3, TMI (Transition metal Ion: Fe(III), Mn(II)) catalyzed O_2 and NO_2. TMI concentrations are prescribed in the model to 0.01 µg m^{-3}

256 for Fe(III) and 0.005 µg m^{-3} for Mn(II) (Martin and Good, 1991). The Fe(III) values are within the

257 range of water soluble iron in winter time aerosol reported in India (Kumar and Sarin, 2010). Wet

258 removal (scavenging), is represented by the (Neu and Prather, 2012) scheme for trace gases and Easter

259 et al., (2004) for aerosols.

260

261 **2.2 Observations**

262   To evaluate the model output, observations of aerosols and meteorology have been obtained

263 from several satellites as well as ground-based measurement platforms. To examine the aerosol

264 loading and spatial and temporal distribution, daily Level 2 Aerosol Optical Depth (AOD) retrievals

265 from the Moderate Resolution Imaging Spectroradiometer (MODIS) aboard Terra and Aqua satellites

266 are obtained at the spatial resolution of 10 km x 10 km (at nadir) pixel array. It provides aerosol

267 properties from the Dark Target (DT) algorithm applied over the ocean and dark land (e.g.,

268 vegetation) and Deep Blue (DB) algorithms over the entire land areas, including both dark and bright

269 surfaces. Each MOD04_L2 (Terra) / MYD04_L2 (Aqua) products are available at a 5-minute time

270 interval with an output grid of 135 pixels in width by 203 pixels in length.

271   The Indian National Satellites (INSAT-3D) in the geostationary orbit at inclinations of 82º

272 longitude provide an imager fog product (3DIMG_L2C_FOG) with a spatial resolution of 4 km every

273 30 min (www.mosdac.gov.in). For daytime, the visible channel observation is used to detect fog,

274 whereas thermal infrared is used to reduce false alarms such as medium/high clouds and snow areas.

275 INSAT 3D's 'day microphysics' data component analyzes solar reflectance at three wavelengths: 0.5

276 µm (visible), 1.6 µm (shortwave infrared), and 10.8 µm (thermal infrared). Night-time fog is derived

277 from TIR-1 (12.0 µm and 10.0 µm) and MIR (10.8 µm and 3.9 µm) channel brightness temperature

278 over the Indian region. INSAT-3D provides fog intensity varying from 1 to 4 indicating SHALLOW

279 for visibility > 600 m; MODERATE, DENSE, and VERY_DENSE, respectively for visibility varying

280 from 0 to 500 m (Banerjee and Padmakumari, 2020). If the visibility is greater than 700 m it indicates

281 no fog while visibility > 1000 m represents very clear skies. Validation of INSAT-3D fog products

282 over the IGP shows a 66%-68% probability of detection and a 10% false alarm rate. It also captures

283 the entire life cycle of fog from formation to dissipation. However, detecting fog during multilayer

284 clouds is still challenging with INSAT-3D (Arun et al., 2018; Chaurasia and Gohil, 2015; Chaurasia

285 and Jenamani, 2017).

286   Ground-based monitoring sites provide hourly data of relative humidity, surface temperature,

287 and wind speed measured by the Central Pollution Control Board, CPCB (http://cpcb.nic.in). Given

288 the data availability from CPCB stations, nine stations have been considered representing each region

289 of IGP, which include, Amritsar, IGI Airport (Indira Gandhi International Airport, Delhi), IHBAS

290 (Institute of Human Behaviour and Allied Sciences, Delhi), Dwarka (Delhi), RKP (Ramakrishna

Puram, Delhi) in the North-West IGP; Kanpur, Lucknow in Central IGP and Patna, Muzaffarpur in East IGP.

In addition, measurements of several aerosols, trace gases, and meteorology at Delhi (IGI Airport) from the Winter Fog Experiment (WiFEX) for the period December 10-31, 2017, have also been used to validate the model output. The WiFEX, an initiative of the Ministry of Earth Sciences (MoES), India, is a ground-based measurement campaign at the IGI Airport Delhi to understand fog's physical and chemical features. Additional details of the WiFEX project and related publications can be found in Ghude et al., (2017).

3 Meteorology Evaluation

Previous studies simulating fog highlight the importance of high model vertical resolution (Pithani et al., 2019; Van Der Velde et al., 2010) for representing the fog formation and the growth of the fog layer, model initialization (Yadav et al., 2022), initial relative humidity (Bergot and Guedalia, 1994; Pithani et al., 2020), and PBL schemes (Chen et al., 2020; Pithani et al., 2019). In the present study, 2-m relative humidity (RH2), 2-m temperature (T2), and 10-m wind speed (WS) from WRF-Chem have been evaluated using ground-based measurements from CPCB monitoring network and WIFEX campaign for nine stations across the IGP. The comparison of WRF-Chem results with observations shows that RH2 and T2 are sensitive to the choice of the meteorological initial and boundary conditions as illustrated by six stations in major cities (Fig. S1). WRF-Chem compares better with the observations for simulations driven by the ERA-Interim reanalysis than with GFS-FNL reanalysis since ERA-Interim provides more realistic RH2 than GFS-FNL (Figs. S2 a-f). For example, RH2 from EXP1 (GFS) varies from 10 to 50%, while RH2 from EXP2 and EXP3 varies from 30 to 100%, which is closer to observation, especially for NWIGP and CIGP. For EIGP, RH2 from EXP1 (GFS) compares better than ERA-Interim, which overestimates the observed RH2. ERA-Interim and YSU PBL scheme showed damping of RH2 continuously increasing the bias in RH2 with time (not shown), which was corrected in EXP2 by refreshing meteorology every day at 00h UT during the model simulation. In addition, maps of surface RH2 and T2 (Figs. S2 g-j) show that the GFS-FNL dataset has lower relative humidity throughout the domain as compared to ERA-Interim. There are differences in simulated 2-m temperature between these two datasets which are of smaller relative magnitude compared to the RH2.

The GFS-FNL driven meteorology EXP1 has a warm bias in NWIGP and CIGP, especially during night-time, while over EIGP, the model prediction agrees well with observations. EXP2 with the ERA-Interim driven meteorology and YSU PBL scheme also shows good agreement between modeled and observed T2 in EIGP. The ERA-Interim driven meteorology with the ACM2 PBL scheme in EXP3 has a cold bias of up to 7ºC over EIGP during daytime from 22nd to 24th December. The wind speed evaluation shows that WRF-Chem is over-predicting wind speed. However, it is also possible that some CPCB stations (e.g., Amritsar and RK Puram) have a wind speed low bias due to

the low measurement height and obstructions such as tall trees near the monitoring station as shown in FigS3. WRF-chem in general overestimates wind speed and several earlier studies have reported this bias in wind speed (e.g., Mohan and Gupta 2018; Pithani et al.,2019). Moreover, WRF-Chem does not have the capability to represent building meteorology and parameterizes the effects of urban areas on meteorology through roughness length, which likely leads to overestimation of wind speed. Note that at other sites (e.g., over IGI-Delhi and Kanpur) the model measurement agreement is better.

The WRF-Chem performance has been statistically assessed against observation using the Taylor Diagram (Taylor, 2001), which provides a statistical summary of how well the model output agrees with the observation in terms of the Pearson correlation, their centered root-mean-square error (RMSE) difference, and the ratios of their variances (Fig. 2). The centered RMS difference is proportional to the distance to point "OBS" in the x-axis which measures the extent to which the simulated and observed datasets match. The centered RMS difference (E'), the correlation (R), and the standard deviations, σ_m^2 (simulated) and σ_o^2 (observed) are calculated as:

$$R = \frac{\frac{1}{N}\sum(M_n - \bar{M})(O_n - \bar{O})}{\sigma_m \sigma_o} \qquad (1)$$

$$E'^2 = \frac{1}{N}\sum[(M_n - \bar{M}) - (O_n - \bar{O})]^2 \qquad (2)$$

$$\sigma_m^2 = \frac{1}{N}\sum(M_n - \bar{M})^2 \qquad (3)$$

$$\sigma_o^2 = \frac{1}{N}\sum(O_n - \bar{O})^2 \qquad (4)$$

where the overall mean of a field is indicated by an overbar.

Each point in the two-dimensional space of the Taylor diagram represents the above mentioned three different statistical metrics simultaneously, as they are related by the follow equation

$$E'^2 = \sigma_o^2 + \sigma_m^2 - 2\sigma_o\sigma_m R \qquad (5)$$

The diagram is constructed based on the similarity of the above equation and the Law of Cosines:

$$c^2 = a^2 + b^2 - 2ab\cos\phi \qquad (6)$$

The percentage bias has also been included to further evaluate the WRF-Chem results. In Fig. 2, better agreement of WRF-Chem results with observations is shown by the marker's proximity to the "OBS" dashed black line. The WRF-Chem RH has a good correlation for all three experiments with r > 0.75 at all the locations in IGP for all the experiments. However, the RMSE (shown by red dashed contours) and the standard deviations are larger for EXP1 compared to EXP2 and EXP3 which lie closer to the dashed black line indicating that the simulated RH variations are similar to observations. The mean bias is also large (>20%) for EXP1 (GFS-FNL) for all the stations, marked by red triangles. For example, simulated RH at Dwarka (4) and Lucknow (7) for EXP2, and IGI Airport (2), IHBAS (3), Lucknow (7), and Patna (8) for EXP3 show good agreement with observation, with r>0.7, standard deviation within ±0.25 and mean bias within 10%. Among these stations, the model performs better for Dwarka (4) and Lucknow (7) for EXP2, IGI Airport (2), and IHBAS (3) for EXP3 with a smaller centered RMSE (<0.75).

363   For all the experiments, WRF-Chem T2 agrees well with observations with a correlation

364   between 0.8 and 0.95. The points are concentrated near the dashed line showing a low RMSE and

365   standard deviation for T2, signifying a good agreement of simulated T2 with observation in terms of

366   temporal variation but the T2 relative bias is large for EXP1 (>20%). The RMSE and relative bias for

367   EXP1 are larger for several of the stations. For example, simulated T2 agrees best with observation at

368   IHBAS (3) for EXP1 and IGI Airport (2) for EXP2, with smaller centered RMSE and standard

369   deviation, and bias <5%. The temporal variability of T2 and RH is predicted well for all the

370   combinations of inputs (Fig. S1), however, the accuracy of simulated T2 and RH is sensitive to the

371   choice of meteorological initial/boundary conditions. WRF-Chem predicted RH and T2 agree better

372   with observations when initialized with ERA-Interim meteorology than with GFS-FNL.

373   The WRF-Chem runs driven by ERA-Interim with YSU (EXP2) and ACM2 PBL (EXP3)

374   schemes predicted the surface meteorology better over the IGP than the WRF-Chem run driven by

375   GFS (EXP1). By examining the modeled cloud water content (averaged over all the grids in the

376   analysis region) in the lowest model level with the INSAT-3D satellite fog intensity for the 23rd and

377   24th December 2017 (Fig. 3), it is apparent that WRF-Chem with the ACM2 PBL scheme compared

378   qualitatively well with observations obtained from INSAT-3D satellite in terms of fog coverage over

379   CIGP, while the WRF-Chem run with the YSU PBL scheme did not produce widespread fog.

380   However, there is also fog over EIGP in WRF-Chem with the ACM2 PBL scheme although it is not

381   observed by the satellite. This is because the model has a cold bias in T2 and a high surface RH over

382   East IGP with ACM2 PBL and Pleim-Xiu surface scheme as discussed earlier, which favors the

383   formation of fog in this region. The time series in Fig. 4 shows that EXP3 is capable of predicting the

384   duration of fog on 23rd and 24th December. There is a data gap from INSAT 3D observations because

385   it is unable to capture fog during daytime in the presence of mid and high-level clouds. Although fog

386   LWC data is available for Delhi from the WiFEx campaign, the WRF-Chem simulation does not

387   produce fog in NWIGP, therefore, the WiFEx observations are not included in this evaluation.

388   In conclusion, EXP3 is the best configuration for predicting fog formation where the ERA-

389   Interim meteorology, the ACM2 PBL and surface schemes, and soil moisture nudging is used in the

390   WRF-Chem simulation. Therefore, the evaluation of predicting AOD, surface aerosol concentrations,

391   and aerosol composition as well as analysis of the impact of aerosols on fog formation uses the EXP3

392   configuration.

393

394   **4   Aerosol Evaluation**

395   Aerosol is an important factor in correct prediction of fog (Maalick et al., 2016; Stolaki et al.,

396   2015) as the number of fog droplets depends on the aerosol size distribution and concentration.

397   Aerosols as CCN can affect the liquid water content in fog and therefore an increase in aerosol

398   concentration can significantly affect fog lifetime (Stolaki et al., 2015; Zhang et al., 2014b). AOD

399   retrievals from the MODIS satellite have been used to validate the modeled AOD (Fig. 5). It is

observed that the model captures several important features of the MODIS retrieved AOD spatial distribution but at the same time somewhat struggles to reproduce the observed AOD magnitude in some parts of the domain. One possible reason for the underestimation would be the EDGAR-HTAP emission inventory, which has a low bias for residential sector $PM_{2.5}$ emissions in India (Sharma et al., 2022). For instance, the model successfully predicts high aerosol loading seen by MODIS on 20 and 21 December over CIGP and EIGP. This is the region with dense fog both in model and observation. Higher AOD (>0.5) over CIGP and EIGP can be attributed to the accumulation of aerosols that are transported by north-westerly winds to these regions from NWIGP (Dey and Di Girolamo, 2011; Jain et al., 2020; Jethva et al., 2018; Kumar et al., 2018; Yadav et al., 2020). However, WRF-Chem underestimates AOD over the NWIGP (AOD<0.3) throughout the simulation period and during 23-24 December over CIGP and EIGP where the latter may be related to enhanced scavenging of aerosols by fog droplets.

The west to east gradient in aerosol loading over IGP is consistent with surface $PM_{2.5}$ distribution (Fig. 6a). Surface $PM_{2.5}$ concentration is highest in EIGP (>100 µg m^{-3}) and it decreases gradually towards NWIGP (~60-80 µg m^{-3}). The time series of $PM_{2.5}$ from CPCB measurements and the model at stations representative of each region in IGP shows that simulated $PM_{2.5}$ compares well with observation in terms of day-to-day variation over most of the locations in the IGP (Fig. 6 b-e). The comparison is good over Amritsar (an NWIGP location), where $PM_{2.5}$ is mostly primary aerosols from local emissions e.g., residential heating related biomass burning. Agricultural waste burning is at its peak during post monsoon months (Oct-Nov), whereas during winter burning for residential heating increases and the stable boundary layer confines these emissions near the surface (Kumar et al., 2021; Pawar and Sinha, 2022). $PM_{2.5}$ at Amritsar shows a bimodal distribution with morning and evening peaks whereas it is absent in the model likely due to the absence of diurnal variations in the WRF-Chem anthropogenic emissions.

At Delhi, the daily variations are predicted well although WRF-Chem underestimates $PM_{2.5}$ observations during the first 4 days. Delhi experiences severe air pollution and haze with high PM loading (> 500 µg m^{-3}) (Bharali et al., 2019). The model is successful in predicting the high $PM_{2.5}$ episode on the 24th of December, but WRF-Chem underpredicts the SO_4^{2-}, NH_4^+, NO_3^- and Cl^- concentrations (Fig. 7). Although simulated SO_2 and NH_3 are comparable with observation, sulfate, and ammonium are underestimated in the model. SO_4^{2-} is underestimated by ~ 9 µg m^{-3}, while NH_4^+, NO_3^- and Cl^- are underestimated by ~30 µg m^{-3}, ~19 µg m^{-3} and ~40 µg m^{-3} on average, respectively. In addition, the WRF-Chem model results show that a large percentage of $PM_{2.5}$ is classified as "other inorganics", which is usually dominated by $PM_{2.5}$ other than BC and OC. The WiFEx observations show that secondary aerosols contribute ~50% of the $PM_{2.5}$ concentration, which is in line with other studies that found secondary aerosols contribute 15-50% to $PM_{2.5}$ mass (Sharma and Mandal, 2017; Behera and Sharma, 2010; Nagar et al., 2017) and NO_3^- constituted 9-13% of $PM_{2.5}$ mass (Lalchandani et al., 2021; Sharma and Mandal, 2017). This leads to the underestimation of $PM_{2.5}$ over Delhi.

437 Studies report very high chloride over the IGP with values exceeding 100 μg m^{-3} (Lalchandani et al.,

438 2021) during winter emitted from increased trash burning and industrial emissions (Pant et al., 2015;

439 Patil et al., 2013). WRF-Chem incorporates trash-burning emissions which include HCl emissions

440 from Chaudhury et al.,(2021) for this study however, the inventory contains annual emissions and fails

441 to resolve the seasonality of trash-burning emissions as identified by Nagpure et al., (2015). They

442 suggested almost all the waste-burning emissions in neighbourhoods with higher socioeconomic status

443 in Delhi occur due to the use of waste as cheap heating fuel by individuals such as night watchmen

444 and pavement dwellers. Chaudhary et al., (2021) considers waste burning that occurs due to lack of

445 collection infrastructure, and at landfills and, therefore, shows a concentration of waste burning

446 emissions around the periphery of Delhi but low waste burning emissions in the relatively prosperous

447 city centre. In addition, emissions from other sources (e.g., industries) are unaccounted for in the

448 model which likely leads to the underestimation in modeled chloride.

449   Over the CIGP and EIGP, the underestimation in PM$_{2.5}$ is mostly observed during the dense

450 fog. It is well known that the hygroscopic aerosols grow in size and are deposited to the surface during

451 fog (Gupta and Mandariya, 2013; Kaul et al., 2011). PM$_{2.5}$ shows an increase initially with the onset

452 of fog and then it decreases as the aerosols grow and get deposited through fog droplets. A two order

453 higher deposition rate (Fig. 6 f, g) during fog compared to the deposition rate of dry aerosol results in

454 the lower PM$_{2.5}$ over CIGP and EICP during fog events.

455   A statistical analysis (Table S1) shows a minimum normalized mean bias (NMB) for PM$_{2.5}$ at

456 Amritsar (2.2%), while in other stations, the normalized mean bias ranges from 48 to 53%, similar to

457 the reported range of model bias (underestimated by 40–60%) in winter over IGP by earlier studies

458 (Bran and Srivastava, 2017; Ojha et al., 2020). This was accomplished by incorporating trash-burning

459 emissions in the model simulation, which improved the PM$_{2.5}$ prediction, increasing NMB by ~4-8%

460 in IGP. RMSE values range from 41 to 138 μg m^{-3} (normalized RMSE~0.4 to 0.7) comparable to the

461 reported values by these studies. The Pearson correlation coefficient (r) for the simulated and observed

462 day-to-day variation in PM$_{2.5}$ lies between 0.4 and 0.7 for all the stations in Fig. 6 except at Patna and

463 Muzaffarpur which lies within the range in these studies. The poor correlation at Patna and

464 Muzaffarpur is due to the low modeled PM$_{2.5}$ concentrations which are caused by increased dry

465 deposition of aerosol particles activated as fog droplets during fog periods, as discussed earlier.

466 Furthermore, the fog events in WRF and observations have somewhat different time periods causing

467 WRF-predicted and the observed PM$_{2.5}$ concentrations to decrease at different times.

468   Previous studies have reported that models tend to underestimate the AOD observation (David

469 et al., 2018; Pan et al., 2015) during the post-monsoon and winter when agricultural waste burning and

470 anthropogenic emissions dominate. While anthropogenic emissions include a contribution from the

471 residential sector, the emissions from small-scale burning for residential heating over IGP especially

472 during winter are likely underestimated in the current emission inventory (Sharma et al., 2022). This

473 leads to an underestimation of aerosol concentration in the model. Other possible causes for the

474   underestimation are the biases in the simulated meteorology (Govardhan et al., 2015; Kumar et al.,

475   2015; Pan et al., 2015) which affects the aerosol concentration. We corrected some of the biases in

476   meteorology as discussed earlier however there are still residual biases in the simulated meteorology

477   e.g., overestimation of wind speed by WRF-Chem. We also observe underestimation of secondary

478   aerosols over NWIGP which contribute significantly to the aerosol loading over IGP. Secondary

479   aerosol formation is substantial over CIGP and EIGP in the model compared to NWIGP which will be

480   discussed in a later section. The underestimation of $PM_{2.5}$ could also be linked to the uncertainty in the

481   model's chemistry scheme to simulate the secondary aerosols due to missing chemical processes or

482   due to underestimation of sulfur oxidation at different RH levels (Acharja et al., 2022; Pawar et al.,

483   2023; Ruan et al., 2022). Moreover, several modeling studies have shown significant improvements in

484   forecasting surface $PM_{2.5}$ by assimilation of satellite AOD and $PM_{2.5}$ (Ghude et al., 2020; Jena et al.,

485   2020; Kumar et al., 2020) suggesting the importance of correct initialization of the model in

486   simulating aerosols over IGP.

487

488   **5**   **Effect of Aerosol Radiation feedback**

489   Interactions of aerosols with radiation affects temperature and surface heat fluxes, thereby

490   weakening the turbulence in the PBL and stabilizing the boundary layer height (Fig. 8b) compared to

491   the clean environment (Fig. 8a). In the presence of well mixed aerosols within the PBL, the radiative

492   effect of aerosols lowers the noontime PBL height (Fig. 8b). However, the presence of absorbing

493   aerosols in the PBL warms the air and changes the thermodynamics. Three cases are shown in Fig.

494   8(c-e) where increases of scattering aerosol concentrations at the top of PBL (Fig. 8c) increases

495   scattering of radiation by the aerosol layer and reduces the surface reaching solar radiation similar to

496   Fig. 8b. Higher concentrations of absorbing aerosols at the top of PBL (Fig. 8d) warms the air above

497   the boundary layer and strengthens the capping inversion stabilizing the PBL and suppressing its

498   growth. The shallow PBL and weakened daytime vertical mixing confines aerosols and water vapor

499   near the surface and worsens the air quality of a region. The aerosols trapped in the stagnant PBL

500   further affects the radiation flux at the surface and creates a positive feedback loop wherein the PBL is

501   continually suppressed until interrupted by some synoptic weather phenomenon, such as the western

502   disturbances in the IGP. On the other hand, higher concentration of absorbing aerosols within the PBL

503   (Fig. 8e) warms the air in the PBL and this results in the higher PBL height. The raised PBL decreases

504   the aerosol concentration near the surface which is termed as a negative feedback effect.

505   The aerosol radiation feedback can affect shortwave heating rates (SWHR). The high aerosol

506   loading over the IGP (Fig. 6 and Fig. 7) allows the AR feedback to reduce the PBL height by more

507   than 140 m throughout the IGP compared to the surrounding region with AR feedback (Fig. 9a). The

508   difference in PBL height with and without aerosol radiation feedback is largest during noontime. The

509   suppressed PBL is due to the decrease in the surface heating flux and the consequent weakening of

510   turbulence in the PBL. The surface solar radiation flux (SWF) decreases by 5-35 % while the surface

latent heat (LH) and sensible heat (HFX) fluxes decrease by 5-35 % and 10-60 %, respectively (Fig. S3). The stable, shallow PBL reduces the vertical mixing of aerosols and moisture and confines them near the surface, resulting in increased $PM_{2.5}$ concentrations and RH near the surface with AR feedback (Fig. 9). Although T2 should decrease with the reduction in surface SWF, T2 shows mixed signals with both cooling and warming over IGP. While surface cooling is observed over NWIGP and EIGP, T2 increases with AR feedback over most of CIGP. The response of AR feedback to T2 varies in these three regions probably due to differences in the distribution and types of aerosols and the presence of fog. Increase in surface concentration of $PM_{2.5}$ occurs more over NWIGP and EIGP with increase in BC and OIN over NWIGP, and sulfate aerosol over EIGP which results in the surface cooling due to positive AR feedback in these two regions. Over the CIGP, the AR feedback causes a depletion of surface $PM_{2.5}$ (Fig. 9d), which is likely due to their hygroscopic growth, and then dry deposition (average $PM_{2.5}$ dry deposition flux of 331 µg m^{-2} hr^{-1} with AR feedback and 282 µg m^{-2} hr^{-1} without AR feedback) in dense fog. The increase in RH with AR feedback favours the growth of aerosols in size by the uptake of water

Examining further, the time variation of the changes in PBL height, T2, and RH between the simulations with and without aerosol-radiation feedback (Fig. 9g) shows an increase in T2 while the surface fluxes, sensible heat flux, latent heat flux, and downward shortwave radiation flux decrease over CIGP (Fig. 9h). AR feedback affects mostly the lower atmosphere at multiple levels; however, our finding suggests that the decreased shortwave radiation flux decreases the surface fluxes and thus the turbulence in the boundary layer resulting in a reduced PBL height on both days. Figure 9 g and h clearly show a decrease in HFX and LH following the decrease in SWF. Moreover, we observe that the PBL height is sensitive to latent heat flux likely due to its strong dependence on moisture availability (Xiu and Pleim, 2001; Zhang and Anthes, 1982).

The impact of AR feedback on T2 depends on factors such as the presence of absorbing aerosols and their vertical distribution via heating or increased SWF (as observed in CIGP, Fig. S4). Absorbing aerosols in WRF-Chem include BC and OIN (other inorganic aerosols), which both increase near the surface (Fig. 9e, Fig. S5) due to their confinement in the stable PBL. Some areas in the fog-affected region show a decrease in BC as well as SO_4^{2-} likely due to increased dry deposition in fog water as discussed earlier in this section for $PM_{2.5}$ As a result, AR feedback changes the absorbing to scattering ratio of aerosols over IGP indicated by the decrease in SSA (Single Scattering Albedo; Fig. S6). In EIGP, sulfate concentrations are larger with AR feedback than without AR feedback with time periods where the difference is >1 µg m^{-3} (Fig.11). The BC concentration changes are small (<0.5 µg m^{-3}) in the EIGP, resulting in a higher SSA near the surface with AR feedback in EIGP. In the CIGP, BC concentrations increase while sulfate aerosols decrease within the PBL with AR feedback (Fig.11) compared to the simulation without AR feedback. A decrease in SSA is seen for the CIGP throughout the boundary layer while in EIGP the decrease occurs near the top of the PBL; difference in SSA due to AR feedback is negligible in NWIGP. Also contributing to the higher SSA in

548   EIGP is the increase in RH (Fig. 9) due to AR feedback favoring the growth of aerosols in size by

549   uptake of water and the production of secondary aerosols such as SO_4^{2-} and NH_4^+.

550   A similar observation has been made by Ramachandran et al., (2020) where SSA decreases

551   with increasing altitude due to absorbing carbonaceous aerosols at higher elevations which contributes

552   $\geq 75\%$ to the aerosol absorption over IGP. Increased shortwave heating (Fig. 10) is probably caused by

553   the increased absorbing aerosols near the surface which overwhelms the surface cooling due to

554   reduced shortwave radiation at the surface.

555   The increase in 2-m RH is substantial over CIGP on 24th December (Fig. 9g) compared to the

556   previous day following the decrease in PBL height which constrains the moisture near the surface.

557   The decrease in RH by 2% or more when aerosol-radiation feedback is included compared to no

558   aerosol-radiation feedback is likely due to increase in T2. However, the increase in RH in the

559   afternoon associated with a decrease in LH and PBL height is important for the air to saturate which

560   then favors the formation of fog in a polluted environment. Note that the increase in T2 with AR

561   feedback is very small ($<0.5°C$) which reduces further after noon (~12:30 pm IST) on both days.

562   Another important factor that can affect the extent of change in PBL height is the distribution

563   of aerosols in the vertical (illustrated in Fig. 8). The pressure-time cross-sections of differences in T,

564   $PM_{2.5}$, BC, and SO_4^{2-} between aerosol radiation (AR) feedback (wFB) and no aerosol radiation

565   feedback (nFB) for three regions, NWIGP, CIGP, and EIGP are shown in Fig. 11. The difference in

566   the PBL height reaches a maximum with the AR feedback during midday (12:30-15:30 IST). Increase

567   in temperature in the boundary layer is observed with AR feedback particularly at the upper PBL in all

568   the regions of IGP. This induces a temperature inversion resulting in a stable and suppressed PBL. In

569   all the regions the decrease in PBL height (100-200 m) is larger on 24th December compared to 23rd

570   December. The difference in the PBL height on 23rd and 24th December with AR feedback on these

571   days is possibly controlled by the aerosol distribution during the previous day or early morning on the

572   same day. For example, in all the regions an increase in $PM_{2.5}$ is observed the previous night (23:30

573   onwards) till ~11:30 of December 24, with increased BC over NWIGP and CIGP whereas both BC

574   and SO_4^{2-} over EIGP. The increased $PM_{2.5}$ concentrations suppress the development of the PBL after

575   sunrise with AR feedback on December 24 compared to that on December 23, leading to the observed

576   differences in ΔPBL height on these two days. Increase in BC concentrations in NWIGP and CIGP are

577   found above the PBL on 24th December whereas BC concentrations decrease within the PBL. This BC

578   concentration gradient creates a temperature inversion, for example between 10:30-14:30 IST. The

579   increase in BC warms the air in the PBL; however, the warming is not strong enough to cause

580   negative feedback over CIGP. On 23rd December a small increase in BC is uniform throughout the

581   PBL, while there is a decrease in SO_4^{2-} concentrations, resulting in a warmer PBL (Fig. 11) with AR

582   feedback.

583   In EIGP, BC distribution is similar to that in CIGP with AR feedback while there is a

584   substantial increase in sulfate aerosol in the PBL. This results in the strongest extinction in EIGP as

585   evident from the largest difference in PBL height and surface cooling with AR feedback among the

586   three regions. Although ΔPBL is small on 23rd December, it still results in the accumulation of

587   aerosols during night-time (~23:30 pm onwards) which further strengthens the AR feedback effect the

588   next day in NWIGP and CIGP. Thus, AR feedback stabilizes the PBL, increases $PM_{2.5}$ and RH in the

589   PBL making conditions favourable for persistence of fog over IGP.

590

591   **6   Effect of Aqueous phase chemistry**

592   In this section we discuss the impact of aqueous phase chemistry on aerosol composition and

593   its interaction with meteorology. There is a considerable difference in the surface concentration of

594     $PM_{2.5}$ (>16 µg m^{-3}) in the absence of aqueous chemistry over CIGP and EIGP where fog occurs (Fig.

595   12a) while the difference is negligible over NWIGP where fog does not occur. This is due to the

596   formation of secondary aerosols through aqueous phase chemistry and the hygroscopic growth of

597   aerosols during fog in these regions with the inclusion of aqueous chemistry in the model. In the

598   region between CIGP and EIGP (83E-84E; marked by the box in Fig. 12a), $PM_{2.5}$ concentration is less

599   in the simulation with aqueous-phase chemistry than without aqueous-phase chemistry because

600   deposition of fog water aerosols to the surface increases as the fog thickens (Fig. 13, Fig. S7). Figure

601   13 shows the relation between formation of secondary aerosols, deposition flux of $PM_{2.5}$, and fog with

602   and without aqueous phase chemistry. During the fog event, the secondary aerosols (SO_4^{2-} , NH_4^+)

603   increase significantly by 4-10 µg m^{-3} due to aqueous phase chemistry adding to the $PM_{2.5}$ burden over

604   IGP. The intensity of fog is high around midnight December 24-25 compared to that on 23rd and 24th

605   (1:30-11:30 IST)) which increases the dry deposition flux of $PM_{2.5}$ causing a sharp drop in the $PM_{2.5}$

606   concentration on 24th December compared to the previous night's fog event. The observed change in

607     $PM_{2.5}$ over a region is the net result of the formation of secondary aerosols and its deposition with fog

608   droplets.

609   The composition distribution of $PM_{2.5}$ (Fig. 12b) has a similar distribution for the simulations

610   with and without aqueous phase chemistry over NWIGP where fog did not occur. The primary

611   aerosols are higher (BC > 9%, OC ~ 16-30%, OIN > 50%), than the secondary aerosols (<5%). While

612   the model requires fog for accelerated formation of secondary inorganic aerosol, experimental data

613   (Fig. 7) supports significant formation of secondary inorganic aerosol at elevated RH levels even in

614   haze aerosol (Acharja et al., 2022). On the other hand, the central and east IGP stations are fog-

615   covered and therefore, there is an increase in secondary aerosols especially SO_4^{2-} and NH_4^+ when

616   aqueous phase chemistry is included in the simulation. SO_4^{2-} is chemically produced via aqueous

617   phase chemistry in cloud water, hence the abrupt increase whereas NH_4^+ maintains a gas-aerosol and

618   gas-cloud equilibrium with NH_3 and SO_4^{2-} via neutralizing the drop or aerosol. NO_3^- is high in the

619   model compared to SO_4^{2-} and NH_4^+ and it decreases by ~1-2 % with aqueous phase chemistry. We

620   observe a small increase in NO_3^- during fog, however it drops as fog intensifies, more rapidly than that

621   without aqueous phase chemistry likely due to increase in dry deposition. This results in lower

622 average NO_3^- to $PM_{2.5}$ ratio with aqueous phase chemistry. Moreover, NO_3^- is high over the fog

623 covered CIGP and EIGP compared to NWIGP suggesting that transport and chemistry of NO_x in

624 CIGP and EIGP produce more HNO_3. Aerosol NO_3^- is also in equilibrium with HNO_3 and it is formed

625 only if excess NH_3 is available beyond the sulfate neutralization. Thus, NH_4^+ and NO_3^- changes are

626 likely due to changing the partitioning between gas and liquid based on the production of sulfate.

627 $PM_{2.5}$ is mostly composed of organic aerosols (OA) over CIGP and EIGP (Lalchandani et al.,

628 2021; Srinivas and Sarin, 2014) whereas $PM_{2.5}$ is OIN (dust) and OA over NWIGP (Ram et al., 2012a;

629 Sharma and Mandal 2023). Although observational studies report Cl^- as one of the largest contributors

630 (12-17%) to $PM_{2.5}$ after the organics (Lalchandani et al., 2021; Pant et al., 2015) during winter, Cl^- is

631 largely underestimated by the model as discussed in section 4 and contributes only ~3%. A small

632 increase (2-4%) in secondary organic aerosols (SOA) from glyoxal production in aerosols occurs for

633 the simulation with aqueous phase chemistry included during intense fog, suggesting there are

634 feedbacks between cloud chemistry (without glyoxal aqueous chemistry) and aerosol chemistry.

635 However, similar to NO_3^-, average SOA (ASOA (anthropogenic)+BSOA (biogenic) + GlySOA)

636 shows a decrease when aqueous phase chemistry is included. SOA contributes significantly to organic

637 aerosol loading over IGP (Kaul et al., 2011; Mandariya et al., 2019).

638 The WRF-Chem results on aerosol composition during fog behave similarly to those of

639 previous observational studies. For example, Ram et al., (2012a) reported an increase of EC, OC, and

640 WSOC concentrations by ~30% during fog and haze events at Allahabad, a location in the Central

641 IGP, and a marginal increase of these constituents at Hisar (NWIGP). Several studies report an

642 increase in inorganic ions (NH_4^+, NO_3^-, and SO_4^{2-}) during fog over IGP and elsewhere (Gundel et al.,

643 1994; Ram et al., 2012a). Recent studies suggest that a significant fraction of atmospheric particulate

644 matter in the IGP is comprised of carbonaceous aerosol (~30–35% of the PM) and water-soluble

645 inorganic species (~10–20% of the PM) during October−January when emissions from biomass

646 burning (including residential heating) are dominant over IGP (Ram et al.,2012b; Rengarajan et al.,

647 2007; Tare et al., 2006).

648 Both the simulations with and without aqueous-phase chemistry include the AR feedback. The

649 aqueous chemistry increases the mass of $PM_{2.5}$ and the size of the aerosols, both of which contribute to

650 AR feedback, thus increasing RH and PBL stability. The increase in RH also saturates the air,

651 promotes aerosol growth by water uptake, and thus favors fog formation. Since the secondary

652 inorganic aerosols are scattering aerosols, the increased scattering of radiation further reduces the

653 solar radiation reaching the surface (Fig. 14a). Over CIGP the presence of higher aerosol loading

654 reduces the T2 during daytime, particularly on the 24th of December which then reduces the PBL

655 height and increases RH near the surface (Fig. 14b). These conditions favor fog formation over the

656 CIGP. Further, the fog water content with aqueous-phase chemistry is higher than that without

657 aqueous-phase chemistry on 24th December post-midnight (Fig. 13b). This is likely due to saturation

658 of air due to increase in RH and lower T2, induced by the AR feedback caused by the increase in

659   PM$_{2.5.}$ Although the difference in T2 is small (<0.4), favourable conditions mentioned above are

660   conducive to fog formation. Because aqueous chemistry increases sulfate concentrations, the size of

661   the aerosols also increase. The increased aerosol size, which can grow further by water uptake, also

662   impacts the solar radiation reaching the surface, affecting fog formation and dissipation.

663

664   **7   Effect of AR feedback and aqueous chemistry on the duration of fog**

665   Aerosol and its radiative effects impact fog characteristics, including the fog liquid water content

666   (LWC), the fog lifetime over a region and hence its spatial and temporal distribution. Variations of fog

667   LWC in WRF-Chem contrast the fog in the CIGP and EIGP (Figure 15) as well as among the three

668   experiments (with aqueous chemistry plus AR feedback, with aqueous chemistry without AR

669   feedback, and without aqueous chemistry but with AR feedback). WRF-Chem does not simulate fog

670   over NWIGP in the model for the study period. In Figure 15, only foggy grid points are considered for

671   the first fog event on 23-24 December. The LWC is 5-15% higher with AR feedback than without AR

672   feedback and without aqueous phase chemistry for both CIGP and EIGP. The interquartile range is

673   larger for the simulation with and without AR feedback than without aqueous phase chemistry in

674   CIGP showing large variability in the LWC. On the other hand, in EIGP the variability in LWC is

675   greater in the simulation with AR feedback compared to the other two experiments.

676   The formation and dissipation times of the two fog events for the three experiments are listed

677   in Tables 2 and 3 for CIGP and EIGP. The 23-24 December fog starts forming two hours earlier and

678   the 24-25 December fog forms one hour earlier in both CIGP and EIGP with AR feedback than

679   without AR feedback. In the simulation without aqueous phase chemistry, fog formation is delayed by

680   an hour or two compared to the simulation with aqueous chemistry plus AR feedback in CIGP. In

681   EIGP the 23-24 December fog forms at the same time with AR feedback and without aqueous phase

682   chemistry while the 24-25 December fog is delayed by an hour without aqueous phase chemistry. Fog

683   dissipation usually occurs after sunrise when the shortwave radiative warming at the surface warms

684   the air, which results in PBL mixing. In addition, absorbing aerosols like BC affect fog dissipation by

685   increasing the radiative heating in and above the fog. We find an increase in BC and shortwave

686   heating in the PBL with AR feedback (Fig. 10,11) and warming over CIGP with AR feedback. Fog

687   intensity starts to decrease after 01:00 UTC (06:30 IST), however, in our study, we find that the fog

688   dissipates completely in the afternoon (~10:00 UTC or 15:30 IST) for both the simulations with AR

689   feedback and no aqueous chemistry while an hour later without AR feedback in CIGP. Fog dissipation

690   is delayed in EIGP with AR feedback compared to that without AR feedback and without aqueous

691   phase chemistry. In both the regions, fog lifetime increases with AR feedback. All the stations,

692   however do not show the same pattern, for example, the 23-24 December fog in Lucknow forms and

693   dissipates at the same time for simulations with AR feedback and without aqueous phase chemistry,

694   and the 24-25 December fog forms later with AR feedback than without AR feedback. Patna shows no

695   difference in the 24-25 December fog formation in all the three experiments. To gain better insights on

696 the fog timing, we recommend that simulations at higher spatial and temporal resolutions be
697 performed to represent better the fog dynamics at point locations. Furthermore, there are other
698 important factors to consider, e.g., improved emissions, better simulations of aerosol chemical
699 composition, and evaluation of aerosol deposition.

700 The AR feedback and aqueous-phase chemistry have the potential to impact aerosol-fog
701 interactions. We can learn about the effect of the aerosol-radiation interactions on CCN concentrations
702 because the WRF-Chem model calculates the CCN concentrations at different supersaturations as a
703 diagnostic output. We compare CCN at 0.02% supersaturations, a value typical of fog, among the
704 three experiments. For the 23-24 December fog in CIGP, hourly CCN concentrations are ~10% higher
705 for the simulations with AR feedback with or without aqueous chemistry than with no AR feedback
706 (Figure S8) during the first 8 hours of the fog event (16:00-24:00 IST 23 December). Surprisingly, the
707 simulation with no aqueous chemistry has higher CCN concentrations than the simulation with
708 aqueous chemistry, as more CCN are expected with aqueous chemistry, because aqueous chemistry
709 adds sulfate to the aerosol mass increasing the mass of $PM_{2.5}$. Increased $PM_{2.5}$ further contributes to
710 AR feedback, increasing RH which favours the growth of the aerosol size, categorizing more aerosols
711 as CCN. However, the dry deposition flux (ddmass) also increases in dense fog which causes rapid
712 loss in CCN and activated aerosols during fog events with the AR feedback (Fig. S7) and more so
713 without aqueous-phase chemistry. Shao et al. (2023) examined aerosol-fog interactions for two
714 consecutive fog events by comparing WRF-Chem results with current emissions strengths to those
715 with low emission strengths. They show that the first fog event promotes formation of the second fog
716 event leading to wider fog distribution, and longer fog lifetime favoured by multiple feedbacks
717 including AR feedback i.e., low temperature, high humidity and high stability similar to our study.
718 While Shao et al. (2023) observe a delay in dissipation of the first event and early formation of second
719 fog event, we find an early dissipation and early formation of fog with AR feedback as discussed
720 earlier in this section. In summary, aqueous phase chemistry together with AR feedback promotes
721 early formation of fog while AR feedback alone promotes early dissipation of fog and plays a critical
722 role in the formation and evolution of the fog over IGP.

723

724   **8 Conclusions**

725 The effects of aerosol-radiation (AR) feedback and aqueous chemistry in air quality and fog
726 have been assessed over IGP. We carried out three experiments using WRF-Chem testing different
727 combinations of PBL schemes and meteorology initial and boundary conditions. The best
728 representation of surface meteorology for the IGP region for the case study (December 20-24, 2017)
729 used ERA-Interim reanalysis to drive the meteorology and ACM2 PBL scheme with soil moisture
730 nudging to ERA-Interim. With this meteorology configuration for WRF-Chem, evaluation of aerosol
731 concentrations with measurements and the impact of aerosols on atmospheric processes during fog
732 were examined. Further, we included trash-burning emissions to represent anthropogenic chloride

aerosols in our configuration. Incorporation of trash burning emissions did improve the model simulations of $PM_{2.5}$ and better captured the day-to-day variability of $PM_{2.5}$ in IGP, yet underestimated its magnitude compared to CPCB observations. Moreover, secondary aerosols particularly, chloride aerosols are underestimated in the model. This underestimation is likely caused by a low bias in the residential burning emission inventory and a failure of the emission inventory to represent residential sector emissions from the use of trash as cheap heating fuel properly. AOD regional distribution is predicted well by the model for most of the IGP. However, AOD is underestimated over NWIGP likely due to an underestimation of fugitive emissions during wintertime cold spells.

The AR interactions showed a significant impact on meteorology and air quality over IGP. A WRF-chem simulation with AR interactions resulted in a lower PBL height by ~50-270 m compared to a simulation without AR interactions leading to accumulation of aerosols and moisture near the surface. Reduced surface shortwave radiation flux and the surface sensible and latent heat fluxes due to aerosol radiative effect suppressed the turbulence resulting in a stable PBL. The shallow PBL further increased surface $PM_{2.5}$ (> 8 µg m^{-3}) and RH (2-8%) over IGP and this positive feedback mechanism promoted thickening of fog over IGP. However, an increase in absorbing aerosols in the PBL gave negative feedback, increasing the shortwave heating and temperature particularly over CIGP. Fog forms when air is saturated which occurs when the surface temperature is reduced or the moisture content increases causing saturation of air. This study suggests that increase in RH saturated the air and the increase in aerosols favoured fog formation as depicted by the thickening of fog intensity. Aqueous phase chemistry on the other hand contributed significantly to secondary aerosols in the fog, especially sulfate aerosols, indicating substantial formation of secondary aerosols in the cloud. The underpredicted secondary aerosols over NWIGP where no fog occurred implies underestimation of formation of aerosols through gas and aerosol chemistry in the model. This underestimation could also be linked to an underestimation of pH in the default MOSAIC scheme (Ruan et al., 2022) which slows the secondary aerosol formation, or an underestimation of the aqueous sulfur oxidation in haze aerosol at > 80% RH before the onset of fog (Acharja et al., 2022), or missing multiphase oxidation processes (Wang et al., 2022). Nevertheless, we find that the model successfully simulates the same changes in the inorganic composition during fog in IGP as reported by observational studies referred earlier in section 6. We also observed that AR feedback with aqueous chemistry initiated the fog formation 1-2 hours earlier than the initiation time in the simulation without AR feedback and without aqueous phase chemistry whereas AR feedback alone led to early dissipation of fog. In addition, fog acted as an important sink of aerosols in a polluted environment with increased dry deposition with cloud water. Thus, AR feedback and aqueous chemistry play a significant role in modulating the distribution and concentration of aerosols and evolution of fog in the PBL. Aerosol-cloud interactions were not investigated in this study due to the limitation of the ACM2 PBL scheme in providing necessary information with other modules in WRF. Previous studies of aerosol-fog interactions have found that ACI also promotes early onset of fog formation and increases

fog duration (Maalick et al., 2016; Yan et al.,2021). While these previous studies were applied to midlatitude fog events, it is likely that ACI also plays a dominant role in IGP fogs, suggesting that future studies are needed to fully understand aerosol effects on IGP fog events.

The large emission of aerosols and trace gases in the IGP makes the atmospheric dynamics as well as chemistry complex, suggesting the need for more studies using both models and ground-based measurements to better understand the processes. While all aerosol types interact with solar radiation and reduce the surface reaching flux, presence of absorbing aerosols in the boundary layer and its vertical distribution plays an important role in modulating the meteorology over IGP. It is therefore crucial to improve the simulation of absorbing aerosols e.g., BC in the vertical as well as at the surface to increase the accuracy in predicting formation as well as the dissipation of fog in this region. Emissions from burning for residential heating are an important source of aerosols in IGP during post-monsoon and winter and the inclusion of these sources in the emission inventory would improve the prediction of wintertime aerosols. For example, the underestimation of chloride aerosol in the model indicates unaccounted emission sources over IGP and the need for more work on better quantifying trash burning emissions, which may not only improve particulate chloride in the model but also improve simulations of other aerosol chemical components through aerosol thermodynamics. Additionally, more detailed modeling studies are required to understand the missing chemical processes if any in the model which leads to biases in sulfate, nitrate and ammonium partitioning between gas and aerosol phases. We find that the change in PBL height with AR feedback is sensitive to changes in LH, signifying the role of soil moisture in PBL dynamics. Several studies have reported cooling over IGP due to an increase in irrigation (Kumar et al., 2017; Mishra et al., 2020). Further investigations into the role of irrigation in the increasing fog events over NWIGP would help in better understanding the formation and persistence of fog over this region. It can be concluded that fog forecasting is a complex process due to the multiple factors involved and this work suggests that AR feedback is important in fog forecasting while aqueous phase chemistry plays an important role in defining the composition of aerosols over IGP.

Acknowledgement

This material is based upon work supported by the NSF National Center for Atmospheric Research (NCAR), which is a major facility sponsored by the U.S. National Science Foundation under Cooperative Agreement No. 1852977. CB is thankful to the Fulbright Kalam Climate Fellowship program under USIEF (United States – India Educational Foundation), and Women Scientist (WOS-A) program, Department of Science and Technology (DST), Govt of India. The authors acknowledge the use of MODIS data from NASA's Land, Atmosphere Near real-time Capability for EOS (LANCE) system (https://earthdata.nasa.gov/lance), part of NASA's Earth Observing System Data and Information System (EOSDIS); Meteorological & Oceanographic Satellite Data Archival Centre

806 (MOSDAC: https://www.mosdac.gov.in/), Space Applications Centre, Indian Space Research
807 Organisation, Govt. of India for INSAT-3D fog data and the Central Pollution Board of India (CPCB:
808 https://app.cpcbccr.com/ccr/#/login) for meteorology data. We would like to acknowledge the high-
809 performance computing support from Cheyenne (doi:10.5065/D6RX99HX) provided by NCAR's
810 Computational and Information Systems Laboratory. We thank Duseong Jo and Behrooz R, and the
811 two anonymous reviewers for their constructive comments on the manuscript.

813 **Data availability:** All the model simulations are archived on the NCAR campaign storage
814 (/glade/campaign/acom/acom-weather/chandrakala) and can be accessed by contacting the
815 corresponding author. WIFEX data can be made available by contacting Dr S.D. Ghude. Trash
816 Burning emission data is available on Mendeley data (doi- http://dx.doi.org/10.17632/t2tn4t9473.1).
817 MODIS AOD retrievals can be downloaded from https://earthdata.nasa. gov/. Meteorology and
818 aerosol data from the Central Pollution Control Board (CPCB) is available at http://cpcb.nic.in.

820 **Author contributions:**

821 CB: Conceptualization, Formal Analysis, Writing

822 MB: Conceptualization, Supervision, Writing-review and editing, Funding acquisition

823 RK: Conceptualization, Supervision, Writing-review and editing

824 SDG: provided ground-based observation data, Writing-review and editing

825 VS and BS: provided trash burning emission data, Writing-review and editing

827 **Competing interests:** The authors declare that they have no conflict of interest.

829 **References**

830 Abdul-Razzak, H. and Ghan, S. J.: A parameterization of aerosol activation 3. Sectional
831 representation, J. Geophys. Res. Atmos., 107(D3), AAC 1-1-AAC 1-6,
832 doi:https://doi.org/10.1029/2001JD000483, 2002.

833 Acharja, P., Ali, K., Ghude, S. D., Sinha, V., Sinha, B., Kulkarni, R., Gultepe, I. and Rajeevan, M. N.:
834 Enhanced secondary aerosol formation driven by excess ammonia during fog episodes in Delhi, India,
835 Chemosphere, 289(July 2021), 133155, doi:10.1016/j.chemosphere.2021.133155, 2022.

836 Arun, S. H., Sharma, S. K., Chaurasia, S., Vaishnav, R. and Kumar, R.: Fog/low clouds detection over
837 the delhi earth station using the ceilometer and the insat-3d/3dr satellite data, Int. J. Remote Sens.,
838 39(12), 4130–4144, doi:10.1080/01431161.2018.1454624, 2018.

839 Badarinath, K. V. S., Kumar Kharol, S. and Rani Sharma, A.: Long-range transport of aerosols from
840 agriculture crop residue burning in Indo-Gangetic Plains—A study using LIDAR, ground
841 measurements and satellite data, J. Atmos. Solar-Terrestrial Phys., 71(1), 112–120,
842 doi:https://doi.org/10.1016/j.jastp.2008.09.035, 2009.

843 Banerjee, S. and Padmakumari, B.: Spatiotemporal variability and evolution of day and night winter

fog over the Indo Gangetic Basin using INSAT-3D and comparison with surface visibility and aerosol optical depth, Sci. Total Environ., 745, 140962, doi:10.1016/j.scitotenv.2020.140962, 2020.

Behera, S. N. and Sharma, M.: Reconstructing primary and secondary components of PM2.5 composition for an Urban Atmosphere, Aerosol Sci. Technol., 44(11), 983–992, doi:10.1080/02786826.2010.504245, 2010.

Bergot, T. and Guedalia, D.: Numerical Forecasting of Radiation Fog. Part I: Numerical Model and Sensitivity Tests, Mon. Weather Rev., 122(6), 1218–1230, doi:10.1175/1520-0493(1994)122<1218:NFORFP>2.0.CO;2, 1994.

Bharali, C., Nair, V. S., Chutia, L. and Babu, S. S.: Modeling of the Effects of Wintertime Aerosols on Boundary Layer Properties Over the Indo Gangetic Plain, J. Geophys. Res. Atmos., 124(7), 4141–4157, doi:10.1029/2018JD029758, 2019.

Bodaballa, J. K., Geresdi, I., Ghude, S. D. and Salma, I.: Numerical simulation of the microphysics and liquid chemical processes occur in fog using size resolving bin scheme, Atmos. Res., 266, 105972, doi:https://doi.org/10.1016/j.atmosres.2021.105972, 2022.

Boutle, I., Price, J., Kudzotsa, I., Kokkola, H. and Romakkaniemi, S.: Aerosol-fog interaction and the transition to well-mixed radiation fog, Atmos. Chem. Phys., 18(11), 7827–7840, doi:10.5194/acp-18-7827-2018, 2018.

Bran, S. H. and Srivastava, R.: Investigation of PM(2.5) mass concentration over India using a regional climate model., Environ. Pollut., 224, 484–493, doi:10.1016/j.envpol.2017.02.030, 2017.

Chapman, E. G., Gustafson, W. I., Easter, R. C., Barnard, J. C., Ghan, S. J., Pekour, M. S. and Fast, J. D.: Coupling aerosol-cloud-radiative processes in the WRF-Chem model: Investigating the radiative impact of elevated point sources, Atmos. Chem. Phys., 9(3), 945–964, doi:10.5194/acp-9-945-2009, 2009.

Chaudhary, P., Garg, S., George, T., Shabin, M., Saha, S., Subodh, S. and Sinha, B.: Underreporting and open burning – the two largest challenges for sustainable waste management in India, Resour. Conserv. Recycl., 175(July), 105865, doi:10.1016/j.resconrec.2021.105865, 2021.

Chaurasia, S. and Gohil, B. S.: Detection of Day Time Fog over India Using INSAT-3D Data, IEEE J. Sel. Top. Appl. Earth Obs. Remote Sens., 8(9), 4524–4530, doi:10.1109/JSTARS.2015.2493000, 2015.

Chaurasia, S. and Jenamani, R. K.: Detection of Fog Using Temporally Consistent, , 10(12), 5307–5313, 2017.

Chen, C., Zhang, M., Perrie, W., Chang, R., Chen, X., Duplessis, P. and Wheeler, M.: Boundary Layer Parameterizations to Simulate Fog Over Atlantic Canada Waters, Earth Sp. Sci., 7(3), doi:10.1029/2019EA000703, 2020.

David, L. M., Ravishankara, A. R., Kodros, J. K., Venkataraman, C., Sadavarte, P., Pierce, J. R., Chaliyakunnel, S. and Millet, D. B.: Aerosol Optical Depth Over India, J. Geophys. Res. Atmos., 123(7), 3688–3703, doi:10.1002/2017JD027719, 2018.

Debnath, S., Karumuri, R. K., Govardhan, G., Jat, R., Saini, H., Vispute, A., Kulkarni, S. H., Jena, C., Kumar, R., Chate, D. M. and Ghude, S. D.: Implications of Implementing Promulgated and Prospective Emission Regulations on Air Quality and Health in India during 2030 N3 - 10.4209/aaqr.220112, AEROSOL AIR Qual. Res. [online] Available from: http://hdl.handle.net/10754/681704, 2022.

Deshpande, P., Meena, D., Tripathi, S., Bhattacharya, A. and Verma, M. K.: Event-based fog climatology and typology for cities in Indo-Gangetic plains, Urban Clim., 51, 101642, doi:https://doi.org/10.1016/j.uclim.2023.101642, 2023.

Dey, S. and Di Girolamo, L.: A decade of change in aerosol properties over the Indian subcontinent, Geophys. Res. Lett., 38(14), 1–5, doi:10.1029/2011GL048153, 2011.

Dey, S. and Tripathi, S. N.: Estimation of aerosol optical properties and radiative effects in the Ganga basin, northern India, during the wintertime, J. Geophys. Res. Atmos., 112(3), doi:10.1029/2006JD007267, 2007.

Dhangar, N. G., Lal, D. M., Ghude, S. D., Kulkarni, R., Parde, A. N., Pithani, P., Niranjan, K., Prasad, D. S. V. V. D., Jena, C., Sajjan, V. S., Prabhakaran, T., Karipot, A. K., Jenamani, R. K., Singh, S. and Rajeevan, M.: On the Conditions for Onset and Development of Fog Over New Delhi: An Observational Study from the WiFEX, Pure Appl. Geophys., 178(9), 3727–3746, doi:10.1007/s00024-021-02800-4, 2021.

Ding, A. J., Huang, X., Nie, W., Sun, J. N., Kerminen, V. M., Petäjä, T., Su, H., Cheng, Y. F., Yang, X. Q., Wang, M. H., Chi, X. G., Wang, J. P., Virkkula, A., Guo, W. D., Yuan, J., Wang, S. Y., Zhang, R. J., Wu, Y. F., Song, Y., Zhu, T., Zilitinkevich, S., Kulmala, M. and Fu, C. B.: Enhanced haze pollution by black carbon in megacities in China, Geophys. Res. Lett., 43(6), 2873–2879, doi:10.1002/2016GL067745, 2016.

Easter, R. C., Ghan, S. J., Zhang, Y., Saylor, R. D., Chapman, E. G., Laulainen, N. S., Abdul-Razzak, H., Leung, L. R., Bian, X. and Zaveri, R. A.: MIRAGE: Model description and evaluation of aerosols and trace gases, J. Geophys. Res. D Atmos., 109(20), doi:10.1029/2004JD004571, 2004.

Emmons, L. K., Schwantes, R. H., Orlando, J. J., Tyndall, G., Kinnison, D., Lamarque, J. F., Marsh, D., Mills, M. J., Tilmes, S., Bardeen, C., Buchholz, R. R., Conley, A., Gettelman, A., Garcia, R., Simpson, I., Blake, D. R., Meinardi, S. and Pétron, G.: The Chemistry Mechanism in the Community Earth System Model Version 2 (CESM2), J. Adv. Model. Earth Syst., 12(4), 1–21, doi:10.1029/2019MS001882, 2020.

Emmons, L. K., Walters, S., Hess, P. G., Lamarque, J. F., Pfister, G. G., Fillmore, D., Granier, C., Guenther, A., Kinnison, D., Laepple, T., Orlando, J., Tie, X., Tyndall, G., Wiedinmyer, C., Baughcum, S. L. and Kloster, S.: Description and evaluation of the Model for Ozone and Related chemical Tracers, version 4 (MOZART-4), Geosci. Model Dev., 3(1), 43–67, doi:10.5194/gmd-3-43-2010, 2010.

Fahey, K. M. and Pandis, S. N.: Optimizing model performance: variable size resolution in cloud chemistry modeling, Atmos. Environ., 35(26), 4471–4478, doi:https://doi.org/10.1016/S1352-2310(01)00224-2, 2001.

Fast, J. D., Gustafson Jr, W. I., Easter, R. C., Zaveri, R. A., Barnard, J. C., Chapman, E. G., Grell, G. A. and Peckham, S. E.: Evolution of ozone, particulates, and aerosol direct forcing in an urban area using a new fully-coupled meteorology, chemistry, and aerosol model, J. Geophys. Res, 111(5), D21305, 2006.

Gautam, R., Hsu, N. C., Kafatos, M. and Tsay, S.: Influences of winter haze on fog / low cloud over the Indo-Gangetic plains, , 112(June 2006), 1–11, doi:10.1029/2005JD007036, 2007.

Ghude, S. D., Bhat, G. S., Prabhakaran, T., Jenamani, R. K., Chate, D. M., Safai, P. D., Karipot, A. K., Konwar, M., Pithani, P., Sinha, V., Rao, P. S. P., Dixit, S. A., Tiwari, S., Todekar, K., Varpe, S., Srivastava, A. K., Bisht, D. S., Murugavel, P., Ali, K., Mina, U., Dharua, M., Jaya Rao, Y.,

Padmakumari, B., Hazra, A., Nigam, N., Shende, U., Lal, D. M., Chandra, B. P., Mishra, A. K., Kumar, A., Hakkim, H., Pawar, H., Acharja, P., Kulkarni, R., Subharthi, C., Balaji, B., Varghese, M., Bera, S. and Rajeevan, M.: Winter fog experiment over the Indo-Gangetic plains of India, Curr. Sci., 112(4), 767–784, doi:10.18520/cs/v112/i04/767-784, 2017.

Ghude, S. D., Chate, D. M., Jena, C., Beig, G., Kumar, R., Barth, M. C., Pfister, G. G., Fadnavis, S. and Pithani, P.: Premature mortality in India due to PM2.5 and ozone exposure, Geophys. Res. Lett., 43(9), 4650–4658, doi:https://doi.org/10.1002/2016GL068949, 2016.

Ghude, S. D., Jenamani, R. K., Kulkarni, R., Wagh, S., Dhangar, N. G., Parde, A. N., Acharja, P., Lonkar, P., Govardhan, G., Yadav, P., Vispute, A., Debnath, S., Lal, D. M., Bisht, D. S., Jena, C., Pawar, P. V., Dhankhar, S. S., Sinha, V., Chate, D. M., Safai, P. D., Nigam, N., Konwar, M., Hazra, A., Dharmaraj, T., Gopalkrishnan, V., Padmakumari, B., Gultepe, I., Biswas, M., Karipot, A. K., Prabhakaran, T., Nanjundiah, R. S. and Rajeevan, M.: WiFEX Walk into the Warm Fog over Indo-Gangetic Plain Region, Bull. Am. Meteorol. Soc., 104(5), E980–E1005, doi:10.1175/BAMS-D-21-0197.1, 2023.

Ghude, S. D., Kulkarni, S. H., Jena, C., Pfister, G. G., Beig, G., Fadnavis, S. and Van Der, R. J.: Application of satellite observations for identifying regions of dominant sources of nitrogen oxides over the indian subcontinent, J. Geophys. Res. Atmos., 118(2), 1075–1089, doi:10.1029/2012JD017811, 2013.

Ghude, S. D., Kumar, R., Jena, C., Debnath, S., Kulkarni, R. G., Alessandrini, S., Biswas, M., Kulkrani, S., Pithani, P., Kelkar, S., Sajjan, V., Chate, D. M., Soni, V. K., Singh, S., Nanjundiah, R. S. and Rajeevan, M.: Evaluation of PM2.5 forecast using chemical data assimilation in the WRF-Chem model: A novel initiative under the Ministry of Earth Sciences Air Quality Early Warning System for Delhi, India, Curr. Sci., 118(11), 1803–1815, doi:10.18520/cs/v118/i11/1803-1815, 2020.

Govardhan, G., Nanjundiah, R. S., Satheesh, S. K., Krishnamoorthy, K. and Kotamarthi, V. R.: Performance of WRF-chem over indian region: Comparison with measurements, J. Earth Syst. Sci., 124(4), 875–896, doi:10.1007/s12040-015-0576-7, 2015.

Grell, G. A., Peckham, S. E., Schmitz, R., McKeen, S. A., Frost, G., Skamarock, W. C. and Eder, B.: Fully coupled "online" chemistry within the WRF model, Atmos. Environ., 39(37), 6957–6975, doi:https://doi.org/10.1016/j.atmosenv.2005.04.027, 2005.

Guenther, A., Karl, T., Harley, P., Weidinmyer, C., Palmer, P. I. and Geron, C.: Edinburgh Research Explorer Estimates of global terrestrial isoprene emissions using MEGAN (Model of Emissions of Gases and Aerosols from Nature) and Physics Estimates of global terrestrial isoprene emissions using MEGAN (Model of Emissions of Gases an, Atmos. Chem. Phys., (6), 3181–3210, 2006.

Gundel, L. A., Benner, W. H. and Hansen, A. D. A.: Chemical composition of fog water and interstitial aerosol in Berkeley, California, Atmos. Environ., 28(16), 2715–2725, doi:https://doi.org/10.1016/1352-2310(94)90443-X, 1994.

Gunwani, P. and Mohan, M.: Sensitivity of WRF model estimates to various PBL parameterizations in different climatic zones over India, Atmos. Res., 194(2016), 43–65, doi:10.1016/j.atmosres.2017.04.026, 2017.

Gupta, T. and Mandariya, A.: Sources of submicron aerosol during fog-dominated wintertime at Kanpur, Environ. Sci. Pollut. Res., 20(8), 5615–5629, doi:10.1007/s11356-013-1580-6, 2013.

Hakkim, H., Sinha, V., Chandra, B. P., Kumar, A., Mishra, A. K., Sinha, B., Sharma, G., Pawar, H., Sohpaul, B., Ghude, S. D., Pithani, P., Kulkarni, R., Jenamani, R. K. and Rajeevan, M.: Volatile

organic compound measurements point to fog-induced biomass burning feedback to air quality in the megacity of Delhi, Sci. Total Environ., 689, 295–304, doi:10.1016/j.scitotenv.2019.06.438, 2019.

Hariprasad, K. B. R. R., Srinivas, C. V., Singh, A. B., Vijaya Bhaskara Rao, S., Baskaran, R. and Venkatraman, B.: Numerical simulation and intercomparison of boundary layer structure with different PBL schemes in WRF using experimental observations at a tropical site, Atmos. Res., 145–146, 27–44, doi:10.1016/j.atmosres.2014.03.023, 2014.

Hong, S. Y., Noh, Y. and Dudhia, J.: A new vertical diffusion package with an explicit treatment of entrainment processes, Mon. Weather Rev., 134(9), 2318–2341, doi:10.1175/MWR3199.1, 2006.

Jacobson, M. Z., Turco, R. P., Jensen, E. J. and Toon, O. B.: Modeling coagulation among particles of different composition and size, Atmos. Environ., 28(7), 1327–1338, doi:https://doi.org/10.1016/1352-2310(94)90280-1, 1994.

Jain, S., Sharma, S. K., Vijayan, N. and Mandal, T. K.: Seasonal characteristics of aerosols (PM2.5 and PM10) and their source apportionment using PMF: A four year study over Delhi, India, Elsevier Ltd., 2020.

Jena, C., Ghude, S. D., Kumar, R., Debnath, S., Govardhan, G., Soni, V. K., Kulkarni, S. H., Beig, G., Nanjundiah, R. S. and Rajeevan, M.: Performance of high resolution (400 m) PM2.5 forecast over Delhi, Sci. Rep., 11(1), 1–9, doi:10.1038/s41598-021-83467-8, 2021.

Jena, C., Ghude, S., Kulkarni, R., Debnath, S., Kumar, R., Soni, V. K., Acharja, P., Kulkarni, S., Khare, M., Kaginalkar, A., Chate, D., Ali, K., Nanjundiah, R. and Rajeevan, M.: Evaluating the sensitivity of fine particulate matter (PM_{2.5}) simulations to chemical mechanism in Delhi, Atmos. Chem. Phys. Discuss., (3), 1–28, 2020.

Jenamani, R. K.: Alarming rise in fog and pollution causing a fall in maximum temperature over Delhi, Curr. Sci., 93(3), 314–322 [online] Available from: http://www.jstor.org/stable/24099461, 2007.

Jethva, H., Chand, D., Torres, O., Gupta, P., Lyapustin, A. and Patadia, F.: Agricultural burning and air quality over northern india: A synergistic analysis using nasa's a-train satellite data and ground measurements, Aerosol Air Qual. Res., 18(7), 1756–1773, doi:10.4209/aaqr.2017.12.0583, 2018.

Katata, G., Chino, M., Kobayashi, T., Terada, H., Ota, M., Nagai, H., Kajino, M., Draxler, R., Hort, M. C., Malo, A., Torii, T. and Sanada, Y.: Detailed source term estimation of the atmospheric release for the Fukushima Daiichi Nuclear Power Station accident by coupling simulations of an atmospheric dispersion model with an improved deposition scheme and oceanic dispersion model, Atmos. Chem. Phys., 15(2), 1029–1070, doi:10.5194/acp-15-1029-2015, 2015.

Kaul, D. S., Gupta, T., Tripathi, S. N., Tare, V. and Collett, J. L.: Secondary organic aerosol: A comparison between foggy and nonfoggy days, Environ. Sci. Technol., 45(17), 7307–7313, doi:10.1021/es201081d, 2011.

Kedia, S., Ramachandran, S., Holben, B. N. and Tripathi, S. N.: Quantification of aerosol type, and sources of aerosols over the Indo-Gangetic Plain, Atmos. Environ., 98, 607–619, doi:10.1016/j.atmosenv.2014.09.022, 2014.

Knote, C., Tuccella, P., Curci, G., Emmons, L., Orlando, J. J., Madronich, S., Baró, R., Jiménez-Guerrero, P., Luecken, D., Hogrefe, C., Forkel, R., Werhahn, J., Hirtl, M., Pérez, J. L., San José, R., Giordano, L., Brunner, D., Yahya, K. and Zhang, Y.: Influence of the choice of gas-phase mechanism on predictions of key gaseous pollutants during the AQMEII phase-2 intercomparison, Atmos. Environ., 115, 553–568, doi:10.1016/j.atmosenv.2014.11.066, 2014.

Krishna Moorthy, K., Suresh Babu, S., Manoj, M. R. and Satheesh, S. K.: Buildup of aerosols over the Indian Region, Geophys. Res. Lett., 40(5), 1011–1014, doi:10.1002/grl.50165, 2013.

Krishna, R. K., Panicker, A. S., Yusuf, A. M. and Ullah, B. G.: On the contribution of particulate matter (PM 2.5) to direct radiative forcing over two urban environments in India, Aerosol Air Qual. Res., 19(2), 399–410, doi:10.4209/aaqr.2018.04.0128, 2019.

Kulkarni, R., Jenamani, R. K., Pithani, P. and Konwar, M.: Loss to Aviation Economy Due to Winter Fog in New Delhi during the Winter of 2011 – 2016, , 1–10, 2019.

Kulkarni, S. H., Ghude, S. D., Jena, C., Karumuri, R. K., Sinha, B., Sinha, V., Kumar, R., Soni, V. K. and Khare, M.: How Much Does Large-Scale Crop Residue Burning Affect the Air Quality in Delhi?, Environ. Sci. Technol., 54(8), 4790–4799, doi:10.1021/acs.est.0c00329, 2020.

Kumar, A. and Sarin, M. M.: Aerosol iron solubility in a semi-arid region: temporal trend and impact of anthropogenic sources, Tellus B, 62(2), doi:10.3402/tellusb.v62i2.16519, 2010.

Kumar, A., Hakkim, H., Sinha, B. and Sinha, V.: Gridded 1 km × 1 km emission inventory for paddy stubble burning emissions over north-west India constrained by measured emission factors of 77 VOCs and district-wise crop yield data, Sci. Total Environ., 789, 148064, doi:10.1016/j.scitotenv.2021.148064, 2021.

Kumar, M., Parmar, K. S., Kumar, D. B., Mhawish, A., Broday, D. M., Mall, R. K. and Banerjee, T.: Long-term aerosol climatology over Indo-Gangetic Plain: Trend, prediction and potential source fields, Atmos. Environ., 180, 37–50, doi:10.1016/j.atmosenv.2018.02.027, 2018.

Kumar, R., Barth, M. C., Pfister, G. G., Nair, V. S., Ghude, S. D. and Ojha, N.: What controls the seasonal cycle of black carbon aerosols in India?, J. Geophys. Res. Atmos., 120(15), 7788–7812, doi:https://doi.org/10.1002/2015JD023298, 2015.

Kumar, R., Ghude, S. D., Biswas, M., Jena, C., Alessandrini, S., Debnath, S., Kulkarni, S., Sperati, S., Soni, V. K., Nanjundiah, R. S. and Rajeevan, M.: Enhancing Accuracy of Air Quality and Temperature Forecasts During Paddy Crop Residue Burning Season in Delhi Via Chemical Data Assimilation., 2020.

Kumar, R., Mishra, V., Buzan, J., Kumar, R., Shindell, D. and Huber, M.: Dominant control of agriculture and irrigation on urban heat island in India, Sci. Rep., 7(1), 1–11, doi:10.1038/s41598-017-14213-2, 2017.

Lalchandani, V., Kumar, V., Tobler, A., M. Thamban, N., Mishra, S., Slowik, J. G., Bhattu, D., Rai, P., Satish, R., Ganguly, D., Tiwari, S., Rastogi, N., Tiwari, S., Močnik, G., Prévôt, A. S. H. and Tripathi, S. N.: Real-time characterization and source apportionment of fine particulate matter in the Delhi megacity area during late winter, Sci. Total Environ., 770, doi:10.1016/j.scitotenv.2021.145324, 2021.

Lelieveld, J., Evans, J. S., Fnais, M., Giannadaki, D. and Pozzer, A.: The contribution of outdoor air pollution sources to premature mortality on a global scale, Nature, 525(7569), 367–371, doi:10.1038/nature15371, 2015.

Ma, Y., Brooks, S. D., Vidaurre, G., Khalizov, A. F., Wang, L. and Zhang, R.: Rapid modification of cloud-nucleating ability of aerosols by biogenic emissions, Geophys. Res. Lett., 40(23), 6293–6297, doi:https://doi.org/10.1002/2013GL057895, 2013.

Maalick, Z., Kühn, T., Korhonen, H., Kokkola, H., Laaksonen, A. and Romakkaniemi, S.: Effect of aerosol concentration and absorbing aerosol on the radiation fog life cycle, Atmos. Environ., 133, 26–

33, doi:10.1016/j.atmosenv.2016.03.018, 2016.

Mandariya, A. K., Gupta, T. and Tripathi, S. N.: Effect of aqueous-phase processing on the formation and evolution of organic aerosol (OA) under different stages of fog life cycles, Atmos. Environ., 206(November 2018), 60–71, doi:10.1016/j.atmosenv.2019.02.047, 2019.

Martin, L. R. and Good, T. W.: Catalyzed oxidation of sulfur dioxide in solution: The iron-manganese synergism, Atmos. Environ. Part A, Gen. Top., 25(10), 2395–2399, doi:10.1016/0960-1686(91)90113-L, 1991.

Mishra, V., Ambika, A. K., Asoka, A., Aadhar, S., Buzan, J., Kumar, R. and Huber, M.: Moist heat stress extremes in India enhanced by irrigation, Nat. Geosci., 13(11), 722–728, doi:10.1038/s41561-020-00650-8, 2020.

Mohan, M. and Bhati, S.: Analysis of WRF Model Performance over Subtropical Region of Delhi, India, Adv. Meteorol., 2011, 1–13, doi:10.1155/2011/621235, 2011.

Mohan, M. and Gupta, M.: Sensitivity of PBL parameterizations on PM10 and ozone simulation using chemical transport model WRF-Chem over a sub-tropical urban airshed in India, Atmos. Environ., 185, 53–63, doi:10.1016/j.atmosenv.2018.04.054, 2018.

Moore, R. H., Cerully, K., Bahreini, R., Brock, C. A., Middlebrook, A. M. and Nenes, A.: Hygroscopicity and composition of California CCN during summer 2010, J. Geophys. Res. Atmos., 117(7), 1–14, doi:10.1029/2011JD017352, 2012.

Nagar, P. K., Singh, D., Sharma, M., Kumar, A., Aneja, V. P., George, M. P., Agarwal, N. and Shukla, S. P.: Characterization of PM2.5 in Delhi: role and impact of secondary aerosol, burning of biomass, and municipal solid waste and crustal matter, Environ. Sci. Pollut. Res., 24(32), 25179–25189, doi:10.1007/s11356-017-0171-3, 2017.

Nagpure, A. S., Ramaswami, A. and Russell, A.: Characterizing the Spatial and Temporal Patterns of Open Burning of Municipal Solid Waste (MSW) in Indian Cities, Environ. Sci. Technol., 49(21), 12904–12912, doi:10.1021/acs.est.5b03243, 2015.

Neu, J. L. and Prather, M. J.: Toward a more physical representation of precipitation scavenging in global chemistry models: Cloud overlap and ice physics and their impact on tropospheric ozone, Atmos. Chem. Phys., 12(7), 3289–3310, doi:10.5194/acp-12-3289-2012, 2012.

Ojha, N., Sharma, A., Kumar, M., Girach, I., Ansari, T. U., Sharma, S. K., Singh, N., Pozzer, A. and Gunthe, S. S.: On the widespread enhancement in fine particulate matter across the Indo-Gangetic Plain towards winter, Sci. Rep., 10(1), 1–9, doi:10.1038/s41598-020-62710-8, 2020.

Pan, X., Chin, M., Gautam, R., Bian, H., Kim, D., Colarco, P. R., Diehl, T. L., Takemura, T., Pozzoli, L., Tsigaridis, K., Bauer, S. and Bellouin, N.: A multi-model evaluation of aerosols over South Asia: Common problems and possible causes, Atmos. Chem. Phys., 15(10), 5903–5928, doi:10.5194/acp-15-5903-2015, 2015.

Pant, P., Shukla, A., Kohl, S. D., Chow, J. C., Watson, J. G. and Harrison, R. M.: Characterization of ambient PM2.5 at a pollution hotspot in New Delhi, India and inference of sources, Atmos. Environ., 109, 178–189, doi:10.1016/j.atmosenv.2015.02.074, 2015.

Patil, R. S., Kumar, R., Menon, R., Shah, M. K. and Sethi, V.: Development of particulate matter speciation profiles for major sources in six cities in India, Atmos. Res., 132–133, 1–11, doi:10.1016/j.atmosres.2013.04.012, 2013.

Pawar, H. and Sinha, B.: Residential heating emissions (can) exceed paddy-residue burning emissions

1099 in rural northwest India, Atmos. Environ., 269, 118846,
1100 doi:https://doi.org/10.1016/j.atmosenv.2021.118846, 2022.

1101 Pawar, P. V., Ghude, S. D., Govardhan, G., Acharja, P., Kulkarni, R., Kumar, R., Sinha, B., Sinha, V.,
1102 Jena, C., Gunwani, P., Adhya, T. K., Nemitz, E. and Sutton, M. A.: Chloride (HCl / Cl-) dominates
1103 inorganic aerosol formation from ammonia in the Indo-Gangetic Plain during winter: modeling and
1104 comparison with observations, Atmos. Chem. Phys., 23(1), 41–59, doi:10.5194/acp-23-41-2023, 2023.

1105 Pithani, P., Ghude, S. D., Chennu, V. N., Kulkarni, R. G., Steeneveld, G. J., Sharma, A., Prabhakaran,
1106 T., Chate, D. M., Gultepe, I., Jenamani, R. K. and Madhavan, R.: WRF Model Prediction of a Dense
1107 Fog Event Occurred During the Winter Fog Experiment (WIFEX), Pure Appl. Geophys., 176(4),
1108 1827–1846, doi:10.1007/s00024-018-2053-0, 2019.

1109 Pithani, P., Ghude, S. D., Jenamani, R. K., Biswas, M., Naidu, C. V., Debnath, S., Kulkarni, R.,
1110 Dhangar, N. G., Jena, C., Hazra, A., Phani, R., Mukhopadhyay, P., Prabhakaran, T., Nanjundiah, R. S.
1111 and Rajeevan, M.: Real-time forecast of dense fog events over Delhi: The performance of the wrf
1112 model during the wifex field campaign, Weather Forecast., 35(2), 739–756, doi:10.1175/WAF-D-19-
1113 0104.1, 2020.

1114 Pleim, J. E. and Chang, J. S.: A non-local closure model for vertical mixing in the convective
1115 boundary layer, Atmos. Environ. Part A. Gen. Top., 26(6), 965–981, doi:https://doi.org/10.1016/0960-
1116 1686(92)90028-J, 1992.

1117 Pleim, J. E. and Gilliam, R.: An indirect data assimilation scheme for deep soil temperature in the
1118 Pleim-Xiu land surface model, J. Appl. Meteorol. Climatol., 48(7), 1362–1376,
1119 doi:10.1175/2009JAMC2053.1, 2009.

1120 Pleim, J. E. and Xiu, A.: Development of a land surface model. Part II: Data assimilation, J. Appl.
1121 Meteorol., 42(12), 1811–1822, doi:10.1175/1520-0450(2003)042<1811:DOALSM>2.0.CO;2, 2003.

1122 Pleim, J. E.: A combined local and nonlocal closure model for the atmospheric boundary layer. Part I:
1123 Model description and testing, J. Appl. Meteorol. Climatol., 46(9), 1383–1395,
1124 doi:10.1175/JAM2539.1, 2007a.

1125 Pleim, J. E.: A combined local and nonlocal closure model for the atmospheric boundary layer. Part II:
1126 Application and evaluation in a mesoscale meteorological model, J. Appl. Meteorol. Climatol., 46(9),
1127 1396–1409, doi:10.1175/JAM2534.1, 2007b.

1128 Powers, J. G., Klemp, J. B., Skamarock, W. C., Davis, C. A., Dudhia, J., Gill, D. O., Coen, J. L.,
1129 Gochis, D. J., Ahmadov, R., Peckham, S. E., Grell, G. A., Michalakes, J., Trahan, S., Benjamin, S. G.,
1130 Alexander, C. R., Dimego, G. J., Wang, W., Schwartz, C. S., Romine, G. S., Liu, Z., Snyder, C.,
1131 Chen, F., Barlage, M. J., Yu, W. and Duda, M. G.: The weather research and forecasting model:
1132 Overview, system efforts, and future directions, Bull. Am. Meteorol. Soc., 98(8), 1717–1737,
1133 doi:10.1175/BAMS-D-15-00308.1, 2017.

1134 Pye, H. O. T., Nenes, A., Alexander, B., Ault, A. P., Barth, M. C., Clegg, S. L., Collett, J. L., Fahey,
1135 K. M., Hennigan, C. J., Herrmann, H., Kanakidou, M., Kelly, J. T., Ku, I. T., Faye McNeill, V.,
1136 Riemer, N., Schaefer, T., Shi, G., Tilgner, A., Walker, J. T., Wang, T., Weber, R., Xing, J., Zaveri, R.
1137 A. and Zuend, A.: The acidity of atmospheric particles and clouds., 2020.

1138 Ram, K., Sarin, M. M. and Tripathi, S. N.: Temporal trends in atmospheric PM 2.5, PM 10, elemental
1139 carbon, organic carbon, water-soluble organic carbon, and optical properties: Impact of biomass
1140 burning emissions in the Indo-Gangetic Plain, Environ. Sci. Technol., 46(2), 686–695,
1141 doi:10.1021/es202857w, 2012b.

Ram, K., Sarin, M. M., Sudheer, A. K. and Rengarajan, R.: Carbonaceous and secondary inorganic aerosols during wintertime fog and haze over urban sites in the Indo-Gangetic plain, Aerosol Air Qual. Res., 12(3), 355–366, doi:10.4209/aaqr.2011.07.0105, 2012a.

Ramachandran, S., Rupakheti, M. and Lawrence, M. G.: Aerosol-induced atmospheric heating rate decreases over South and East Asia as a result of changing content and composition, Sci. Rep., 10(1), 1–17, doi:10.1038/s41598-020-76936-z, 2020.

Rengarajan, R., Sarin, M. M. and Sudheer, A. K.: Carbonaceous and inorganic species in atmospheric aerosols during wintertime over urban and high-altitude sites in North India, J. Geophys. Res. Atmos., 112(21), 1–16, doi:10.1029/2006JD008150, 2007.

Ruan, X., Zhao, C., Zaveri, R. A., He, P., Wang, X., Shao, J. and Geng, L.: Simulations of aerosol pH in China using WRF-Chem (v4 . 0): sensitivities of aerosol pH and its temporal variations during haze episodes, , 6143–6164, 2022.

Safai, P. D., Ghude, S., Pithani, P., Varpe, S., Kulkarni, R., Todekar, K., Tiwari, S., Chate, D. M., Prabhakaran, T., Jenamani, R. K. and Rajeevan, M. N.: Two-way relationship between aerosols and fog: A case study at IGI airport, New Delhi, Aerosol Air Qual. Res., 19(1), 71–79, doi:10.4209/aaqr.2017.11.0542, 2019.

Sarkar, C., Roy, A., Chatterjee, A., Ghosh, S. K. and Raha, S.: Factors controlling the long-term (2009–2015) trend of PM2.5 and black carbon aerosols at eastern Himalaya, India, Sci. Total Environ., 656, 280–296, doi:10.1016/j.scitotenv.2018.11.367, 2019.

Sarkar, S., Chokngamwong, R., Cervone, G., Singh, R. P. and Kafatos, M.: Variability of aerosol optical depth and aerosol forcing over India, Adv. Sp. Res., 37(12), 2153–2159, doi:10.1016/j.asr.2005.09.043, 2006.

Sengupta, A., Govardhan, G., Debnath, S., Yadav, P., Kulkarni, S. H., Parde, A. N., Lonkar, P., Dhangar, N., Gunwani, P., Wagh, S., Nivdange, S., Jena, C., Kumar, R. and Ghude, S. D.: Probing into the wintertime meteorology and particulate matter (PM2.5 and PM10) forecast over Delhi, Atmos. Pollut. Res., 13(6), 101426, doi:https://doi.org/10.1016/j.apr.2022.101426, 2022.

Shao, N., Lu, C., Jia, X., Wang, Y., Li, Y., Yin, Y., Zhu, B., Zhao, T., Liu, D., Niu, S., Fan, S., Yan, S. and Lv, J.: Self-enhanced aerosol – fog interactions in two successive radiation fog events in the Yangtze River Delta , China : A simulation study, , (January), 1–46, 2023.

Sharma, A. R., Kharol, S. K., Badarinath, K. V. S. and Singh, D.: Impact of agriculture crop residue burning on atmospheric aerosol loading - A study over Punjab State, India, Ann. Geophys., 28(2), 367–379, doi:10.5194/angeo-28-367-2010, 2010.

Sharma, G., Annadate, S. and Sinha, B.: Will open waste burning become India ' s largest air pollution source ? ☆, Environ. Pollut., 292(PA), 118310, doi:10.1016/j.envpol.2021.118310, 2022.

Sharma, S. K. and Mandal, T. K.: Chemical composition of fine mode particulate matter (PM2.5) in an urban area of Delhi, India and its source apportionment, Urban Clim., 21, 106–122, doi:10.1016/j.uclim.2017.05.009, 2017.

Sharma, S. K. and Mandal, T. K.: Elemental Composition and Sources of Fine Particulate Matter (PM2.5) in Delhi, India, Bull. Environ. Contam. Toxicol., 110(3), 1–8, doi:10.1007/s00128-023-03707-7, 2023.

1182 Shin, H. H. and Hong, S. Y.: Intercomparison of Planetary Boundary-Layer Parametrizations in the
1183 WRF Model for a Single Day from CASES-99, Boundary-Layer Meteorol., 139(2), 261–281,
1184 doi:10.1007/s10546-010-9583-z, 2011.

1185 Singh, A. and Dey, S.: Influence of aerosol composition on visibility in megacity Delhi, Atmos.
1186 Environ., 62, 367–373, doi:10.1016/j.atmosenv.2012.08.048, 2012.

1187 Singh, N., Banerjee, T., Raju, M. P., Deboudt, K., Sorek-Hamer, M., Singh, R. S. and Mall, R. K.:
1188 Aerosol chemistry, transport, and climatic implications during extreme biomass burning emissions
1189 over the Indo-Gangetic Plain, Atmos. Chem. Phys., 18(19), 14197–14215, doi:10.5194/acp-18-14197-
1190 2018, 2018.

1191 Srinivas, B. and Sarin, M. M.: PM2.5, EC and OC in atmospheric outflow from the Indo-Gangetic
1192 Plain: Temporal variability and aerosol organic carbon-to-organic mass conversion factor, Sci. Total
1193 Environ., 487(1), 196–205, doi:10.1016/j.scitotenv.2014.04.002, 2014.

1194 Srivastava, P., Dey, S., Srivastava, A. K., Singh, S. and Tiwari, S.: Most probable mixing state of
1195 aerosols in Delhi NCR, northern India, Atmos. Res., 200(September 2017), 88–96,
1196 doi:10.1016/j.atmosres.2017.09.018, 2018.

1197 Steeneveld, G. J., Ronda, R. J. and Holtslag, A. A. M.: The Challenge of Forecasting the Onset and
1198 Development of Radiation Fog Using Mesoscale Atmospheric Models, Boundary-Layer Meteorol.,
1199 154(2), 265–289, doi:10.1007/s10546-014-9973-8, 2015.

1200 Stolaki, S., Haeffelin, M., Lac, C., Dupont, J. C., Elias, T. and Masson, V.: Influence of aerosols on
1201 the life cycle of a radiation fog event. A numerical and observational study, Atmos. Res., 151, 146–
1202 161, doi:10.1016/j.atmosres.2014.04.013, 2015.

1203 Syed, F. S., Körnich, H. and Tjernström, M.: On the fog variability over south Asia, Clim. Dyn.,
1204 39(12), 2993–3005, doi:10.1007/s00382-012-1414-0, 2012.

1205 Tare, V., Tripathi, S. N., Chinnam, N., Srivastava, A. K., Dey, S., Manar, M., Kanawade, V. P.,
1206 Agarwal, A., Kishore, S., Lal, R. B. and Sharma, M.: Measurements of atmospheric parameters during
1207 Indian Space Research Organization Geosphere Biosphere Program Land Campaign II at a typical
1208 location in the Ganga basin: 2. Chemical properties, J. Geophys. Res. Atmos., 111(23),
1209 doi:10.1029/2006JD007279, 2006.

1210 Tav, J., Masson, O., Burnet, F., Paulat, P., Bourrianne, T., Conil, S. and Pourcelot, L.: Determination
1211 of fog-droplet deposition velocity from a simple weighing method, Aerosol Air Qual. Res., 18(1),
1212 103–113, doi:10.4209/aaqr.2016.11.0519, 2018.

1213 Taylor, K. E.: in a Single Diagram, , 106, 7183–7192, 2001.

1214 Van Der Velde, I. R., Steeneveld, G. J., Wichers Schreur, B. G. J. and Holtslag, A. A. M.: Modeling
1215 and forecasting the onset and duration of severe radiation fog under frost conditions, Mon. Weather
1216 Rev., 138(11), 4237–4253, doi:10.1175/2010MWR3427.1, 2010.

1217 Verma, S., Ramana, M. V. and Kumar, R.: Atmospheric rivers fueling the intensification of fog and
1218 haze over Indo-Gangetic Plains, Sci. Rep., 12(1), 1–9, doi:10.1038/s41598-022-09206-9, 2022.

1219 Wang, T., Liu, M., Liu, M., Song, Y., Xu, Z., Shang, F., Huang, X., Liao, W., Wang, W., Ge, M., Cao,
1220 J., Hu, J., Tang, G., Pan, Y., Hu, M. and Zhu, T.: Sulfate Formation Apportionment during Winter
1221 Haze Events in North China, Environ. Sci. Technol., 56(12), 7771–7778, doi:10.1021/acs.est.2c02533,
1222 2022.

1223 Wexler, A. S., Lurmann, F. W. and Seinfeld, J. H.: Modelling urban and regional aerosols—I. model

development, Atmos. Environ., 28(3), 531–546, doi:https://doi.org/10.1016/1352-2310(94)90129-5, 1994.

Wiedinmyer, C., Akagi, S. K., Yokelson, R. J., Emmons, L. K., Al-Saadi, J. A., Orlando, J. J. and Soja, A. J.: The Fire INventory from NCAR (FINN): A high resolution global model to estimate the emissions from open burning, Geosci. Model Dev., 4(3), 625–641, doi:10.5194/gmd-4-625-2011, 2011.

Xie, B., Fung, J. C. H., Chan, A. and Lau, A.: Evaluation of nonlocal and local planetary boundary layer schemes in the WRF model, J. Geophys. Res. Atmos., 117(12), 1–26, doi:10.1029/2011JD017080, 2012.

Xiu, A. and Pleim, J. E.: Development of a land surface model. Part I: Application in a mesoscale meteorological model, J. Appl. Meteorol., 40(2), 192–209, doi:10.1175/1520-0450(2001)040<0192:DOALSM>2.0.CO;2, 2001.

Yadav, P., Parde, A. N., Dhangar, N. G., Govardhan, G., Lal, D. M., Wagh, S., Prasad, D. S. V. V. D., Ahmed, R. and Ghude, S. D.: Understanding the genesis of a dense fog event over Delhi using observations and high-resolution model experiments, Model. Earth Syst. Environ., doi:10.1007/s40808-022-01463-x, 2022.

Yadav, R., Bhatti, M. S., Kansal, S. K., Das, L., Gilhotra, V., Sugha, A., Hingmire, D., Yadav, S., Tandon, A., Bhatti, R., Goel, A. and Mandal, T. K.: Comparison of ambient air pollution levels of Amritsar during foggy conditions with that of five major north Indian cities: multivariate analysis and air mass back trajectories, SN Appl. Sci., 2(11), 1–11, doi:10.1007/s42452-020-03569-2, 2020.

Yan, S., Zhu, B., Zhu, T., Shi, C. and Liu, D.: The Effect of Aerosols on Fog Lifetime : Observational Evidence and Model Simulations Geophysical Research Letters, , 1–10, doi:10.1029/2020GL091156, 2021.

Yu, H., Liu, S. C. and Dickinson, R. E.: Radiative effects of aerosols on the evolution of the atmospheric boundary layer, J. Geophys. Res. Atmos., 107(12), doi:10.1029/2001jd000754, 2002.

Zaveri, R. A., Easter, R. C. and Peters, L. K.: A computationally efficient Multicomponent Equilibrium Solver for Aerosols (MESA), J. Geophys. Res. Atmos., 110(24), 1–22, doi:10.1029/2004JD005618, 2005.

Zaveri, R. A., Easter, R. C., Fast, J. D. and Peters, L. K.: Model for Simulating Aerosol Interactions and Chemistry (MOSAIC), J. Geophys. Res. Atmos., 113(13), 1–29, doi:10.1029/2007JD008782, 2008.

Zhang, D. and Anthes, R. A.: A High-Resolution Model of the Planetary Boundary Layer—Sensitivity Tests and Comparisons with SESAME-79 Data, J. Appl. Meteorol. Climatol., 21(11), 1594–1609, doi:10.1175/1520-0450(1982)021<1594:AHRMOT>2.0.CO;2, 1982.

Zhang, F., Li, Y., Li, Z., Sun, L., Li, R., Zhao, C., Wang, P., Sun, Y., Liu, X., Li, J., Li, P., Ren, G. and Fan, T.: Aerosol hygroscopicity and cloud condensation nuclei activity during the AC3Exp campaign: Implications for cloud condensation nuclei parameterization, Atmos. Chem. Phys., 14(24), 13423–13437, doi:10.5194/acp-14-13423-2014, 2014a.

Zhang, X., Musson-Genon, L., Dupont, E., Milliez, M. and Carissimo, B.: On the Influence of a Simple Microphysics Parametrization on Radiation Fog Modelling: A Case Study During ParisFog, Boundary-Layer Meteorol., 151(2), 293–315, doi:10.1007/s10546-013-9894-y, 2014b.

1266

1267

1268

1269 Table 1 Experiment set-up for the study. Numbers in parentheses for the physics options denote the
1270 namelist settings of the WRF-Chem model.

1271

	EXP 1	EXP 2	EXP 3
Meteorology Initial /lateral boundary Condition:	*NCEP Final Analysis (GFS-FNL), 1° x1°, 6 hourly*	*ERA-Interim Project, 1.125° x 0.703°, 6 hourly*	*ERA-Interim Project, 1.125° x 0.703°, 6 hourly*
Physics Options			
Cloud Physics	*Morrison 2-mom (10)*	*Morrison 2- mom (10)*	*Morrison 2- mom (10)*
Longwave Radiation	*RRTMG scheme (4)*	*RRTMG scheme (4)*	*RRTMG scheme (4)*
Shortwave Radiation	*Goddard shortwave (2)*	*RRTMG scheme (4)*	*RRTMG scheme (4)*
Surface Layer Physics	*Revised MM5 Monin-Obukhov scheme (1)*	*Revised MM5 Monin-Obukhov scheme (1)*	*Pleim-Xiu (7)*
Surface Model	*unified Noah land-surface model (2)*	*NoahMP (4)*	*Pleim-Xiu (7)*
PBL Scheme	*YSU scheme (1)*	*YSU (1)*	*ACM2 (7)*
Convective Parameterization	*Grell-Freitas (3)*	*Grell-Freitas (3)*	*Grell-Freitas (3)*
	Continuous simulation	**Meteorology refreshed every 24 hr*	***Continuous simulation: Soil nudging included*

1272
1273
1274
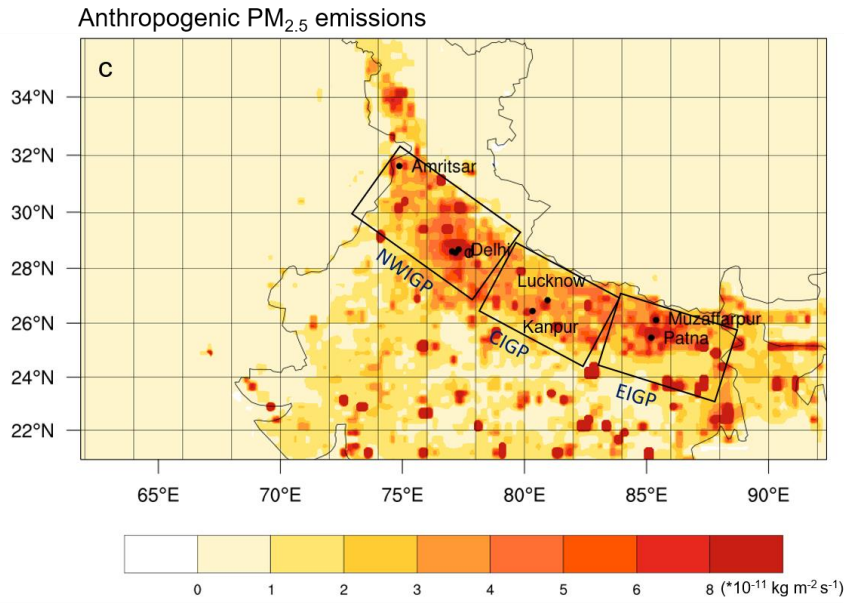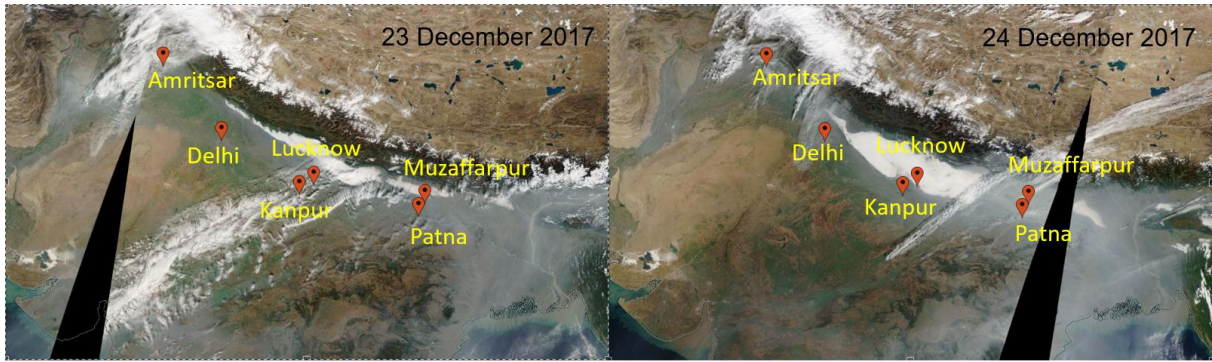
1275

Figure 1 The MODIS reflectance (true color) map representing low cloud over Indo Gangetic Plains, India (study region) indicative of likely fog and haze on 23rd December (a) and 24th December (b) 2017. (c) Anthropogenic emission of $PM_{2.5}$ over IGP for December 2017 obtained from EDGAR-HTAP. The boxes represent the regions Northwest IGP (NWIGP), Central IGP (CIGP), and East IGP (EIGP).

1281

1282
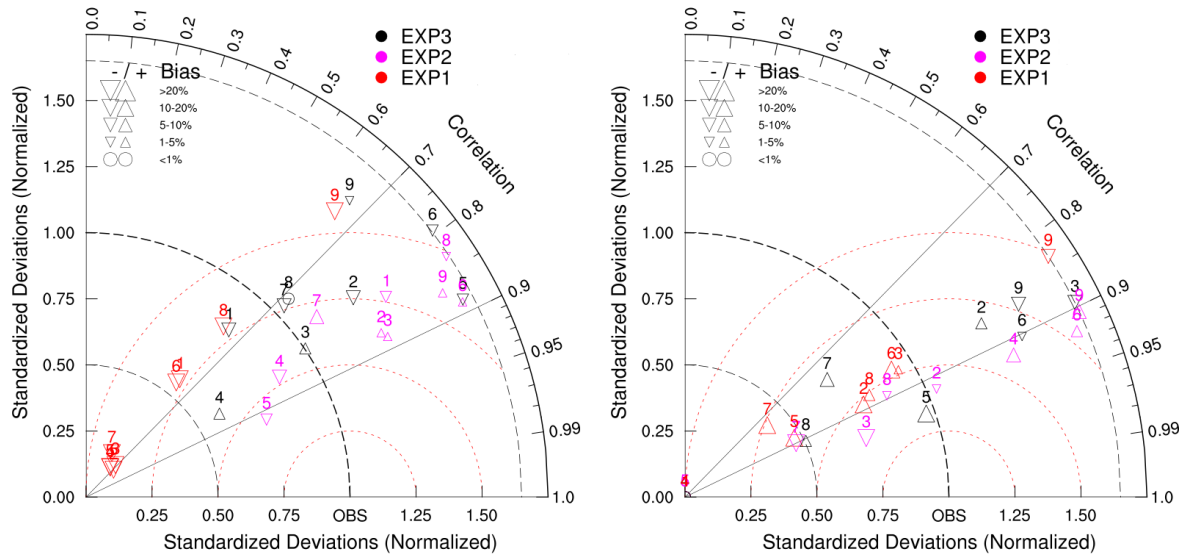
1283

1284 Figure 2 Taylor Diagram of simulated (WRF-Chem) and observed (CPCB) relative humidity (left) and

1285 2-m temperature (right) over IGP. The colors indicate the experiments. The red dotted contours

1286 represent RMS values. The marker (triangles) size varies with a mean bias between the experiments

1287 and observation. Upside-down triangles represent positive bias (exp-obs) and vice versa. The stations

1288 over IGP are denoted by number 1. Amritsar, 2. IGI Airport (Delhi), 3. IHBAS (Delhi), 4. Dwarka

1289 (Delhi), 5. RKP (Delhi), 6. Kanpur, 7. Lucknow, 8. Patna, 9. Muzaffarpur. The locations are marked

1290 in Fig.1a.

1291
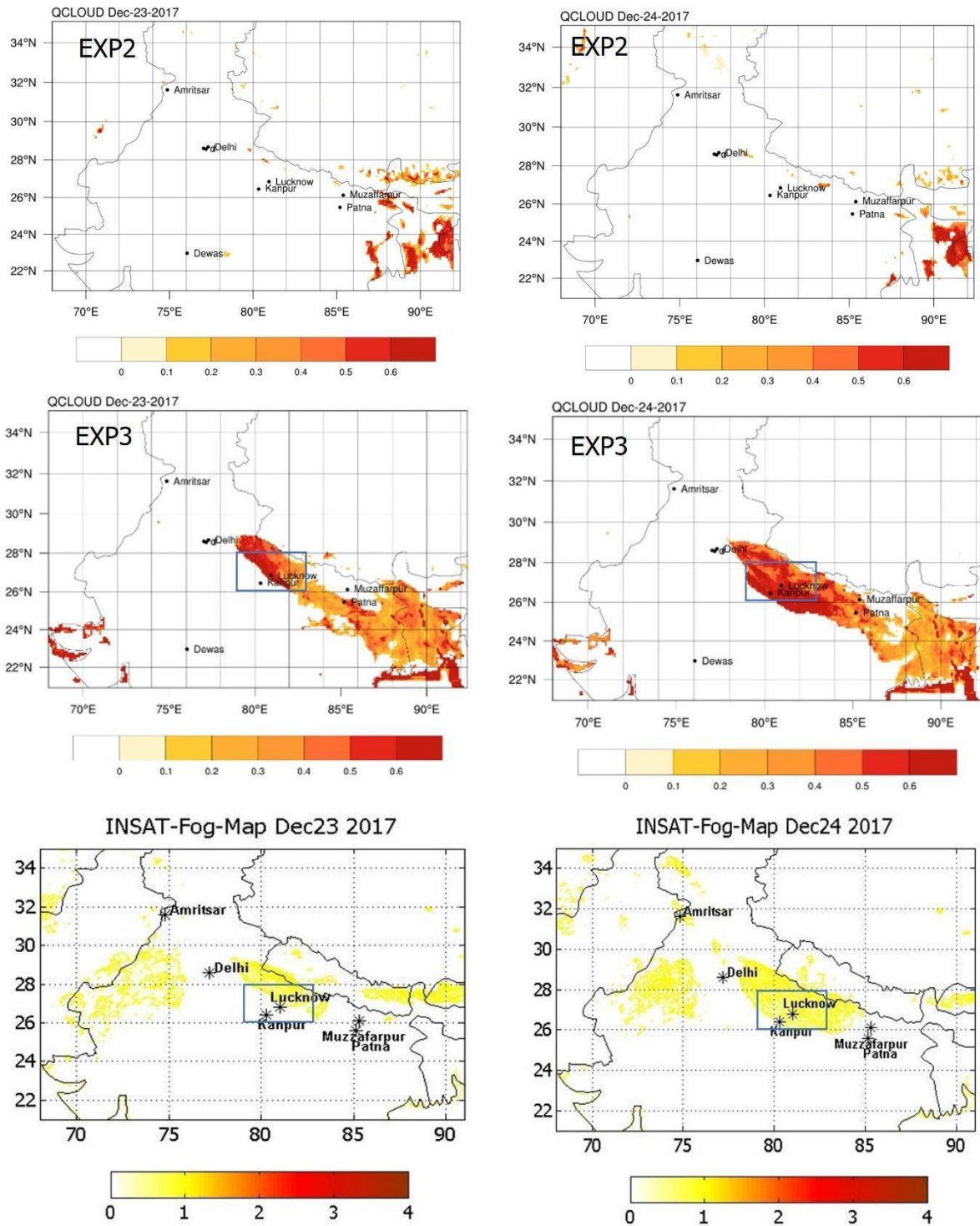
1292

Figure 3 Average WRF-Chem surface layer cloud water mixing ratios (g m^{-3}) for EXP2 and EXP3

(top four panels) and INSAT-3D satellite fog intensity (bottom two panels) on 23 and 24 December

2017. INSAT-3D satellite fog intensity varies from 0 to 4 indicating SHALLOW, MODERATE,

DENSE, and VERY_DENSE, respectively. The rectangle in central IGP is the region for the time

series analysis.

1298
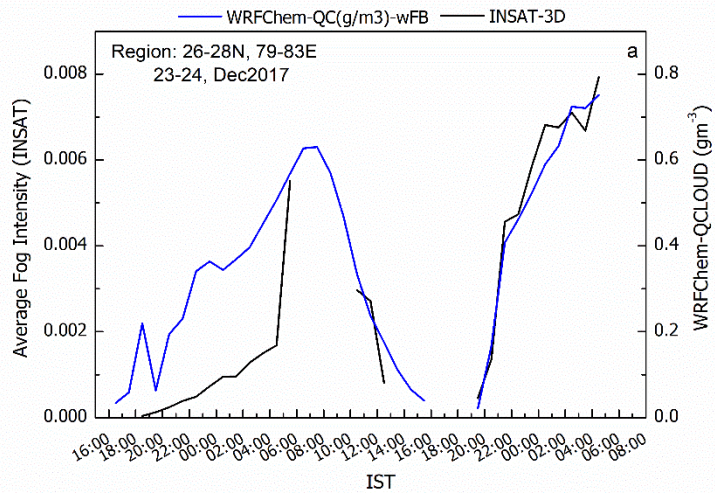
1299

Figure 4 Average Hourly variation of fog on 23 and 24 December 2017 from WRF-Chem EXP3

simulation and INSAT-3D satellite between 26°N-28°N,79°E-83°E (region shown in Fig 3). The time

is in IST (Indian Standard Time; IST is 5.5 hours ahead of Universal Time Coordinate (UTC).

1303
1304
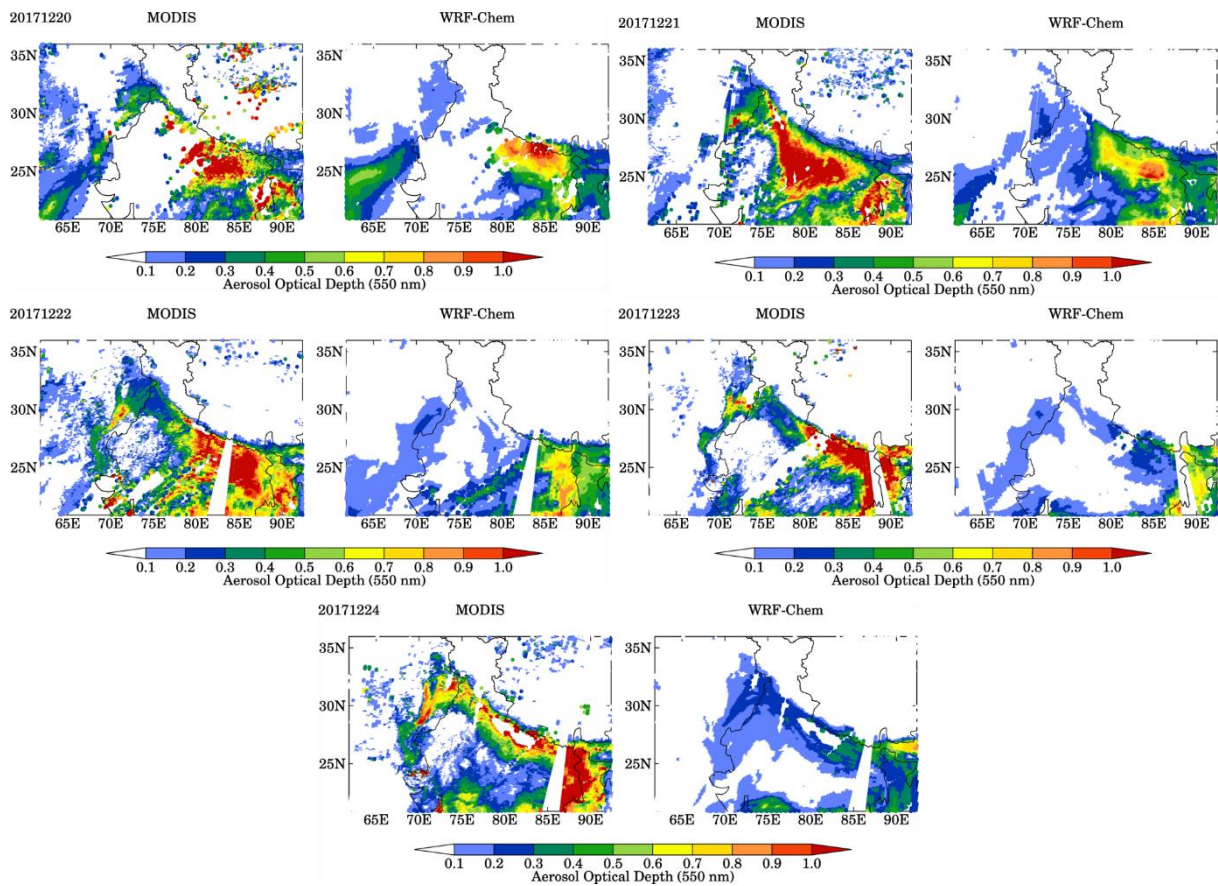
1305

Figure 5 Comparison of WRF-Chem AOD with MODIS observation over the model domain on 20,
21, 22, 23, and 24 December 2017.

1308

1309   .
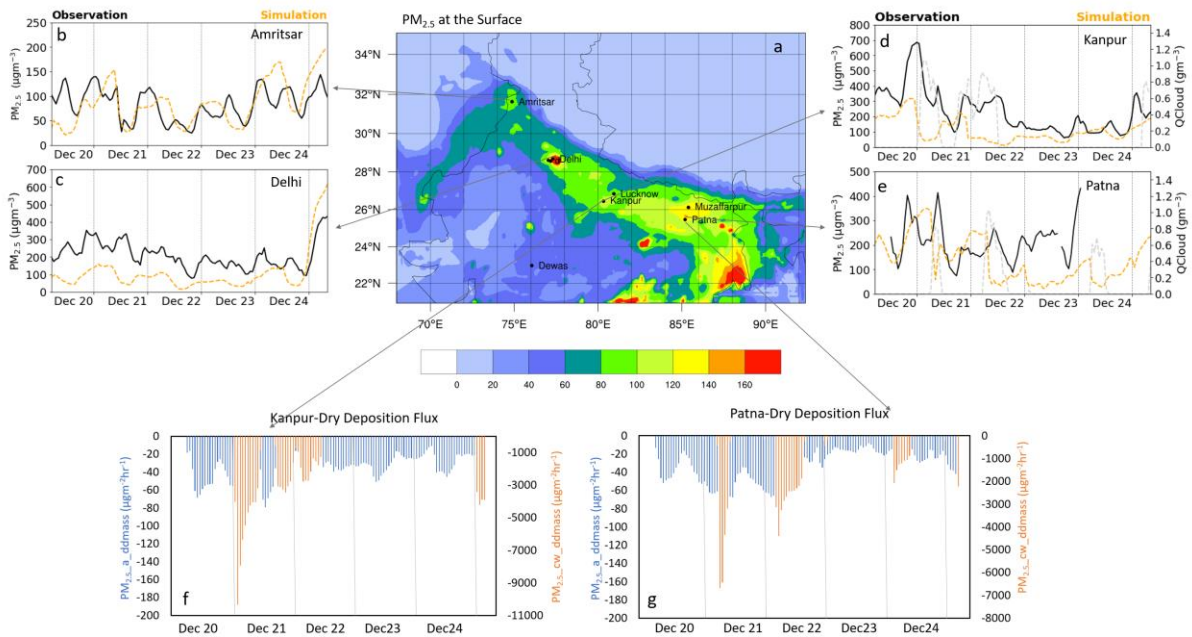
1312 Figure 6 WRF-Chem simulated surface PM$_{2.5}$ map over IGP (a); comparison of WRF-Chem PM$_{2.5}$

1313 with CPCB observation for the period 20-24 Dec 2017 for (b) Amritsar, (c) Delhi, (d) Kanpur and (e)

1314 Patna. Dry Deposition rate of PM$_{2.5}$ for (f) Kanpur and (g) Patna. The grey dotted line in (d) Kanpur

1315 and (e) Patna is fog (QCloud) present during the study period.
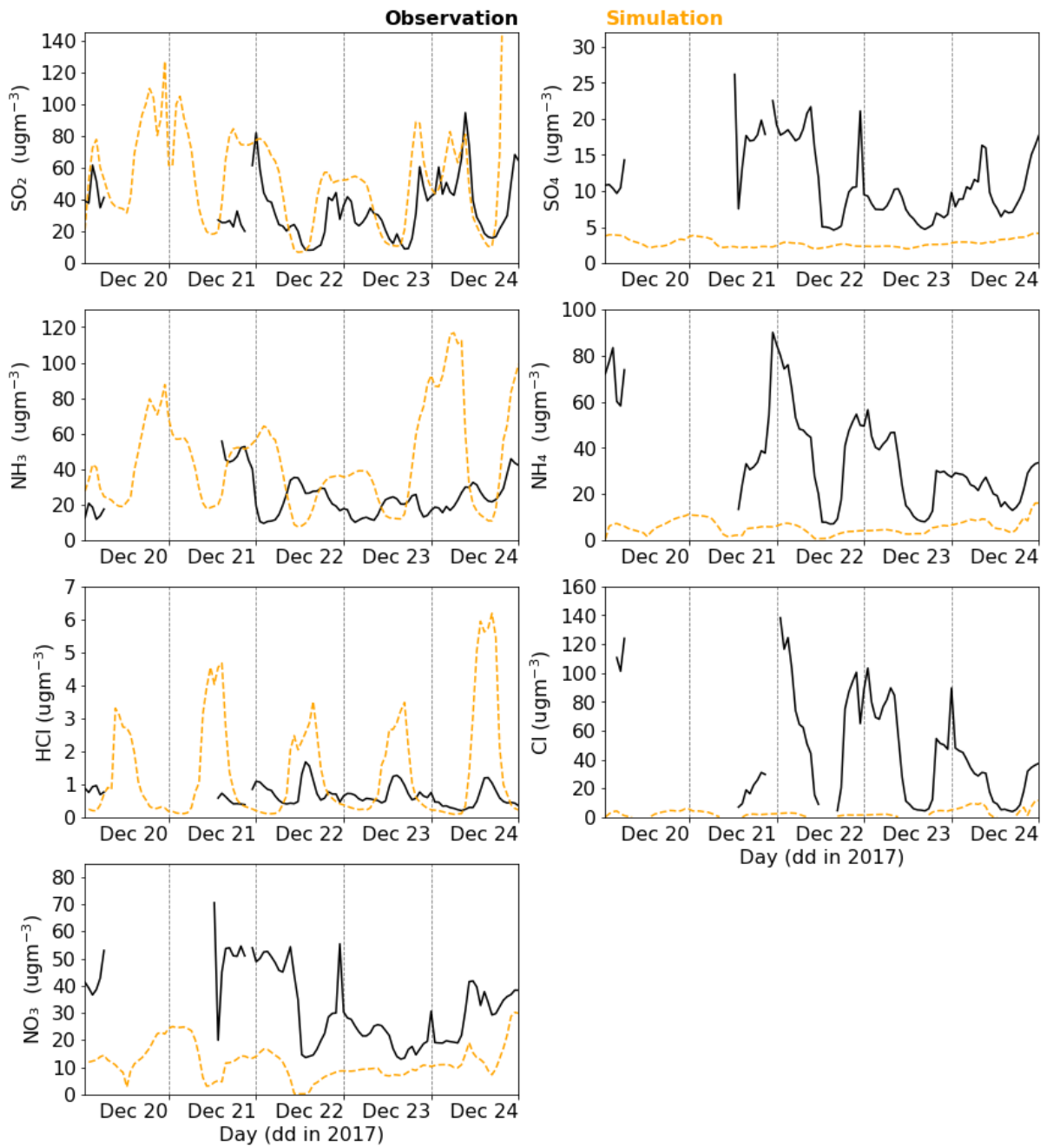
1317

1318   Figure 7 Comparison of WRF-Chem simulated ions (SO_4^{2-}, NH_4^+, NO_3^-, Cl^-) and trace gases (SO_2,

1319 NH_3 & HCl) with the observation from WIFEX campaign at Delhi.

1320

1321

1322
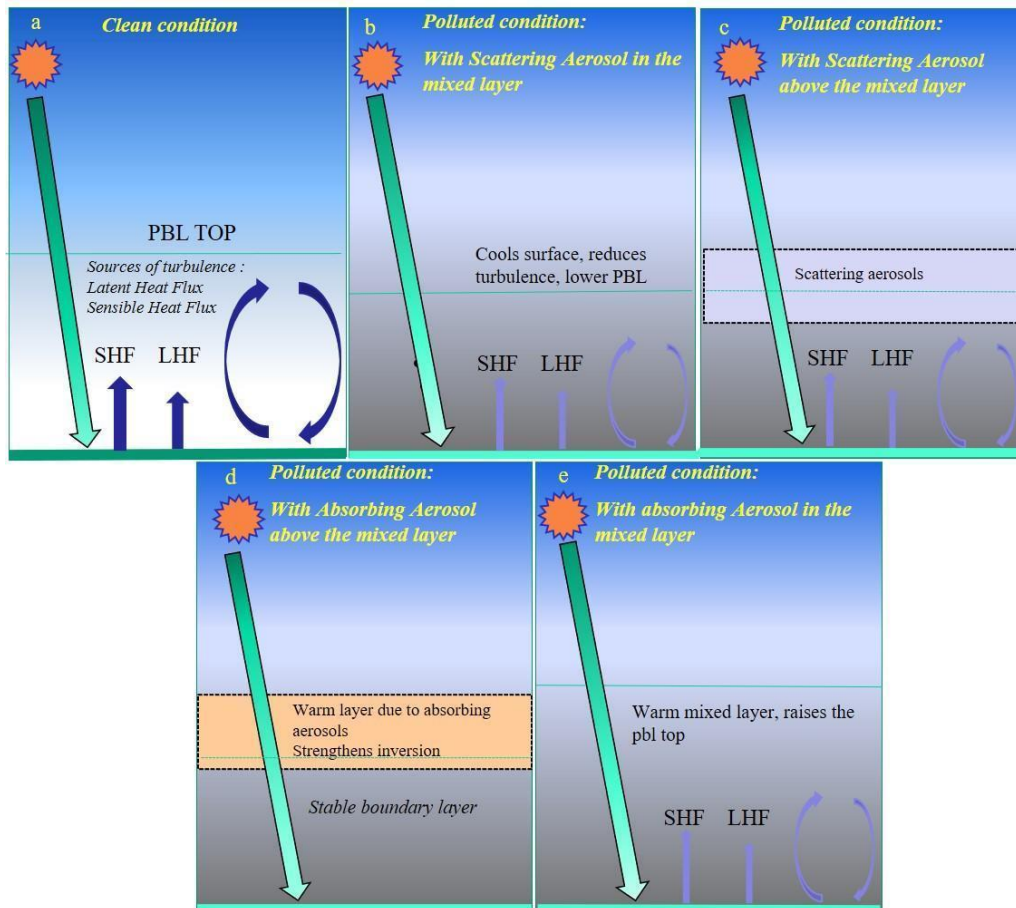
1323

1324   Figure 8 Schematic diagram of Aerosol Radiation Feedback.

1325

1326

1327
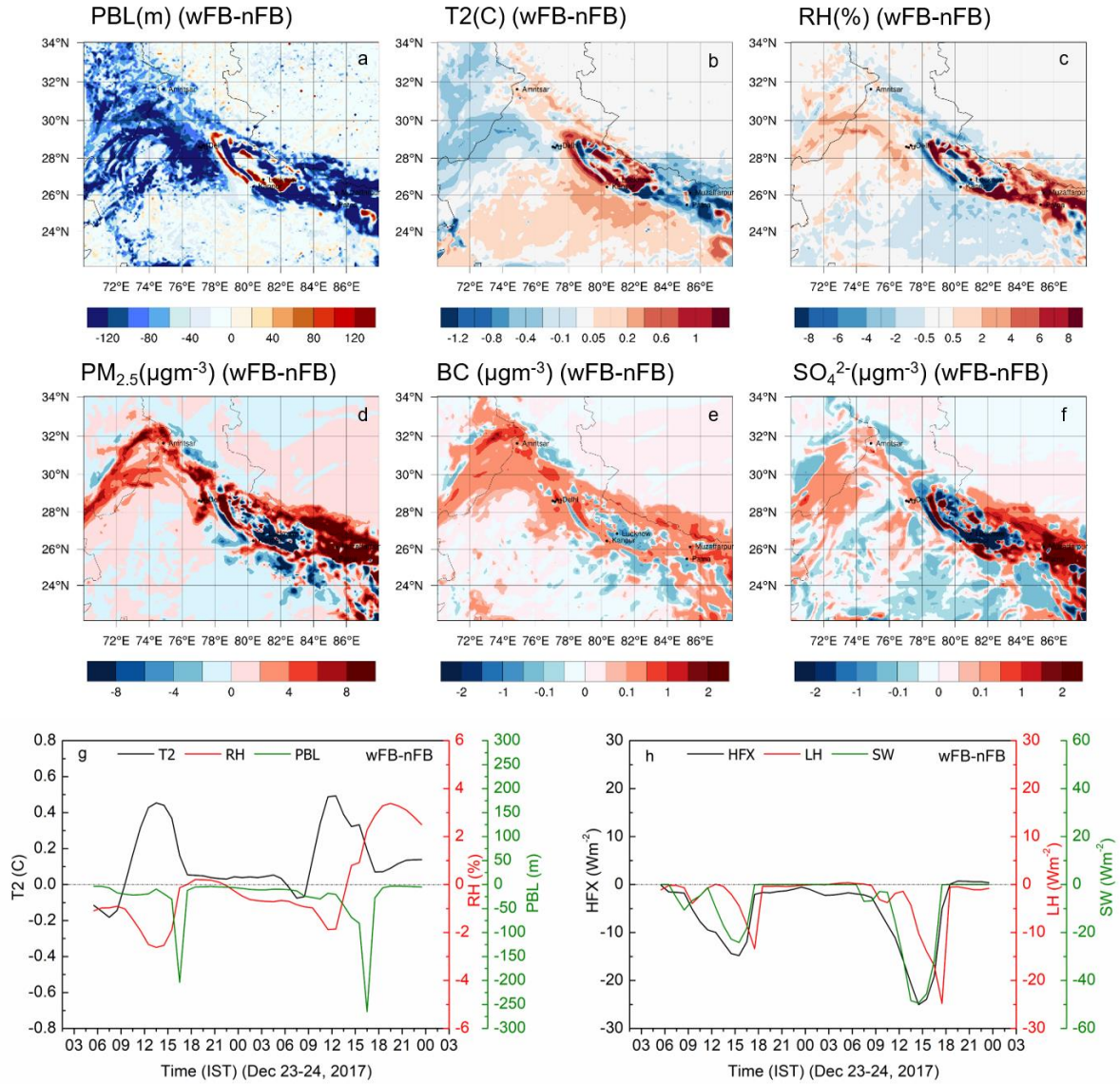
1328

1329 Figure 9 Effect of Aerosol Radiation feedback (wFB-nFB) on (a) PBL height, (b) 2-m temperature, (c)

1330 2-m relative humidity, (d) surface PM$_{2.5}$, (e) surface BC and (f) surface SO$_4$ for December 24 at local

1331 noon (13:30-15:30 IST). (g) The time series of ΔPBL, ΔT2, and ΔRH; (h) ΔHFX (sensible heat flux),

1332 ΔLH (latent heat flux), and ΔSWF (downward shortwave flux) over CIGP for December 23 and 24. Δ

1333 denotes the difference between with and without AR feedback (wFB-nFB).

1334
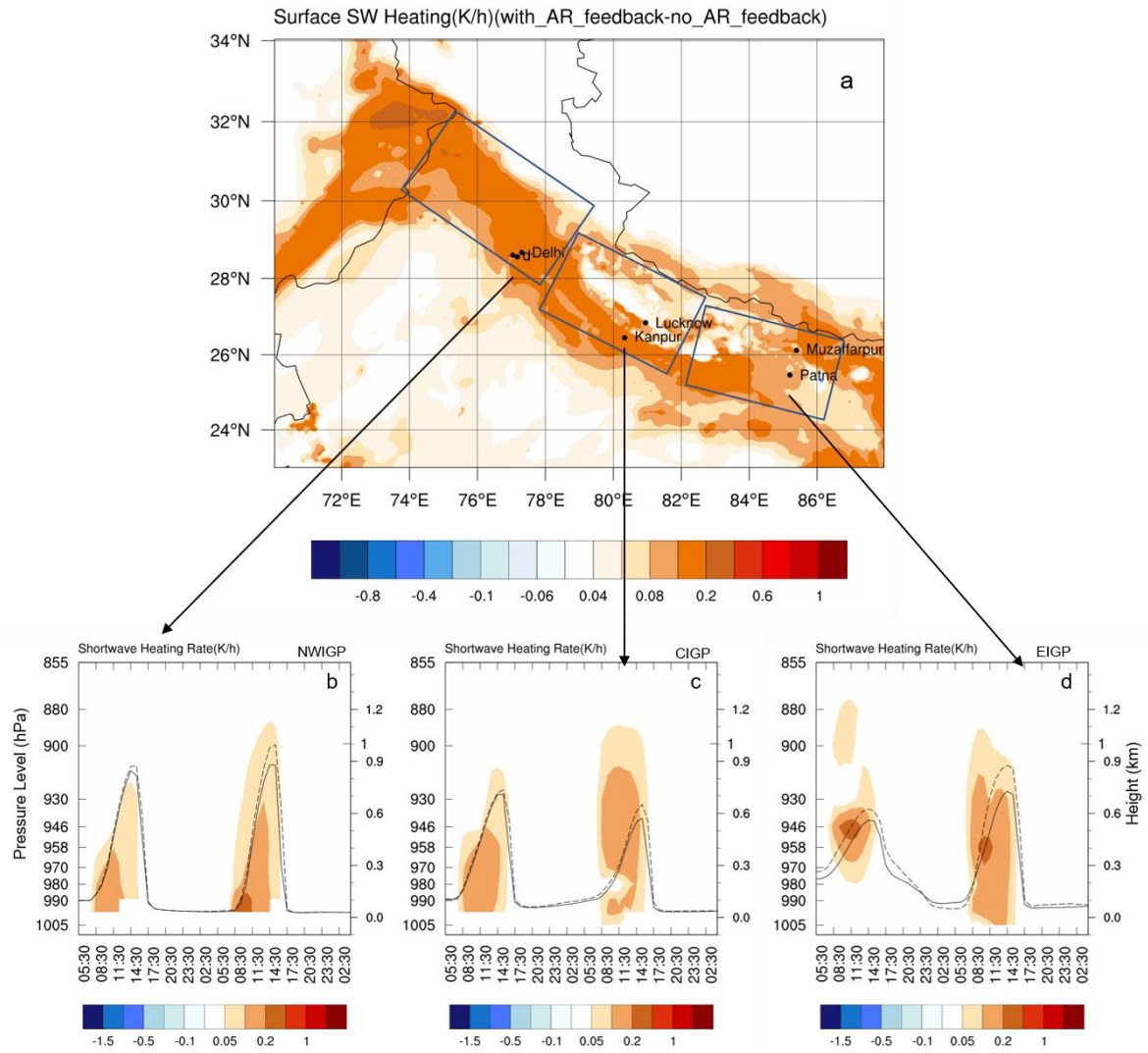
1335
1336

Figure 10 Differences in shortwave heating rates (K h^{-1}) between simulations with and without aerosol radiation feedback (a) at the surface, and for pressure-time cross-sections over (b) NWIGP, (c) CIGP. And (d) EIGP for December 23 and 24. The solid and dashed lines are the PBL height with and without AR feedback respectively. The time is in IST.
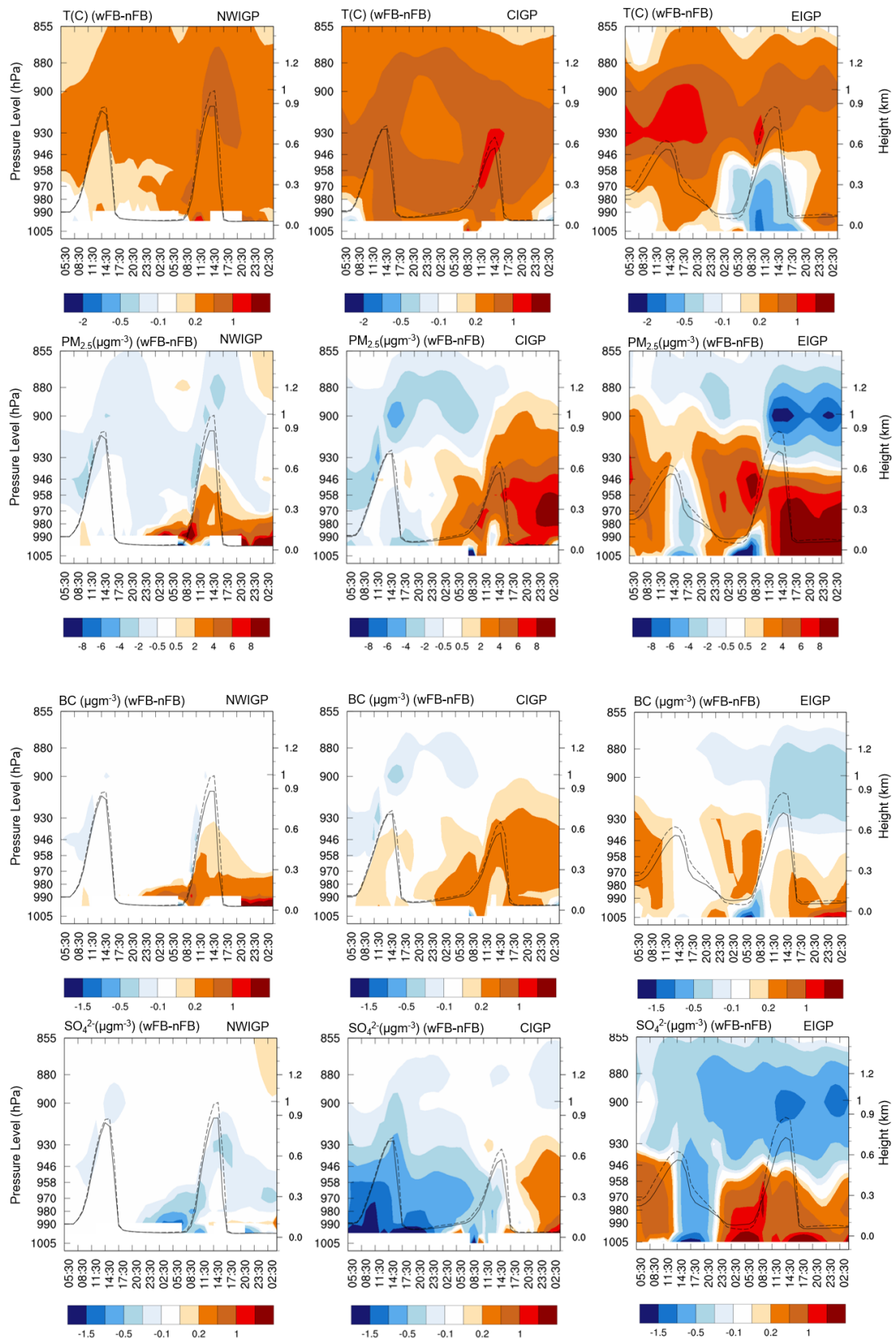
1341

1342

1343

1344 Figure 11 Pressure-time cross-section of the differences in T, PM$_{2.5}$, BC and SO$_4^{2-}$ between

1345 simulations with and without the AR feedback for December 23 and 24. The solid and dashed lines

1346 are the PBL height with and without AR feedback respectively. The time is in IST.

1347

1348
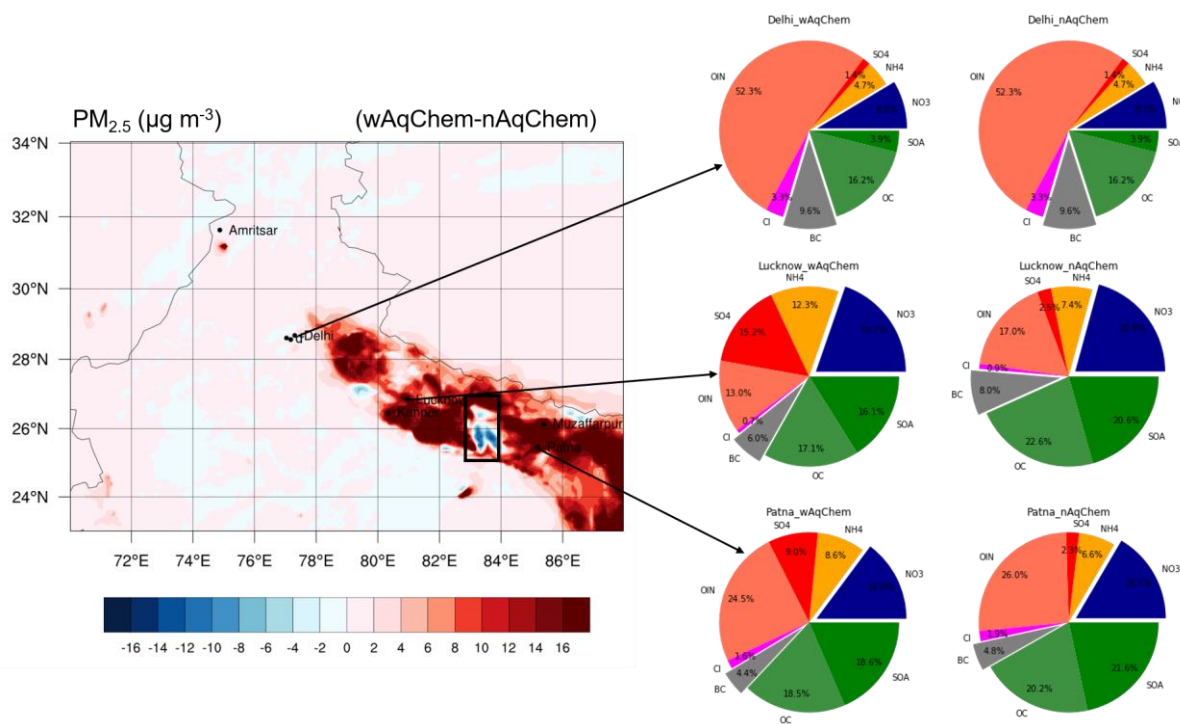
1349

1350 Figure 12 (a) Surface ΔPM$_{2.5}$ (wAq.chem-noAq.chem) and (b) pie charts of PM$_{2.5}$ composition

1351 distribution for the two cases, with and without Aqueous phase Chemistry for 24 Dec 2017. The

1352 stations Delhi, Lucknow (LKN), and Patna are representative of NWIGP, CIGP, and EIGP regions

1353 respectively.

1354

1355

1356
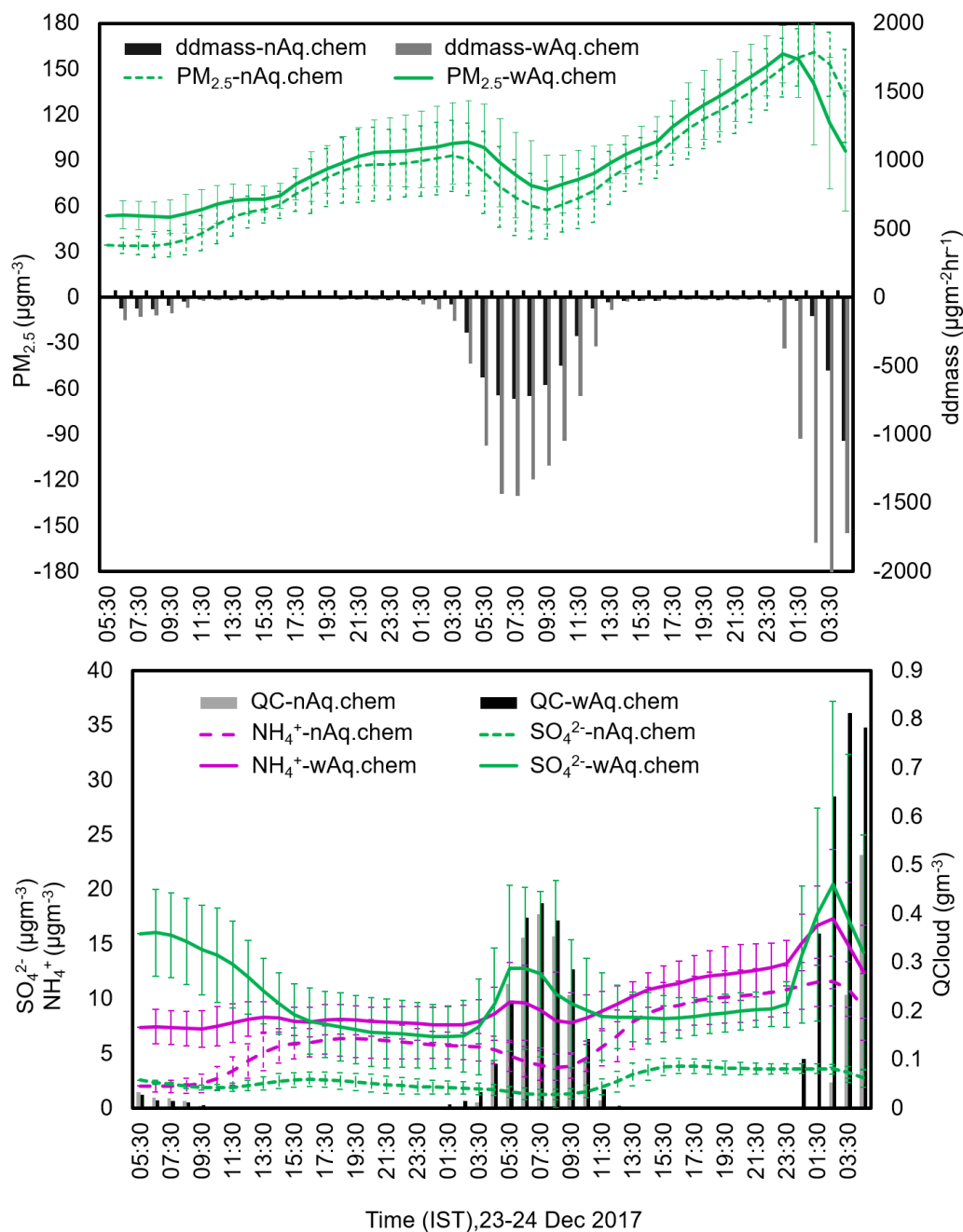
1357

1358   Figure 13 Time series of (a) $PM_{2.5}$ and its dry deposition (ddmass) flux change, (b) SO_4^{2-}, NH_4^+ and

1359   LWC (QCloud) with and without aqueous phase chemistry included in the model, averaged over the

1360   region bounded by a black rectangle in Fig. 12, for 23 and 24 December, 2017.

1361

1362
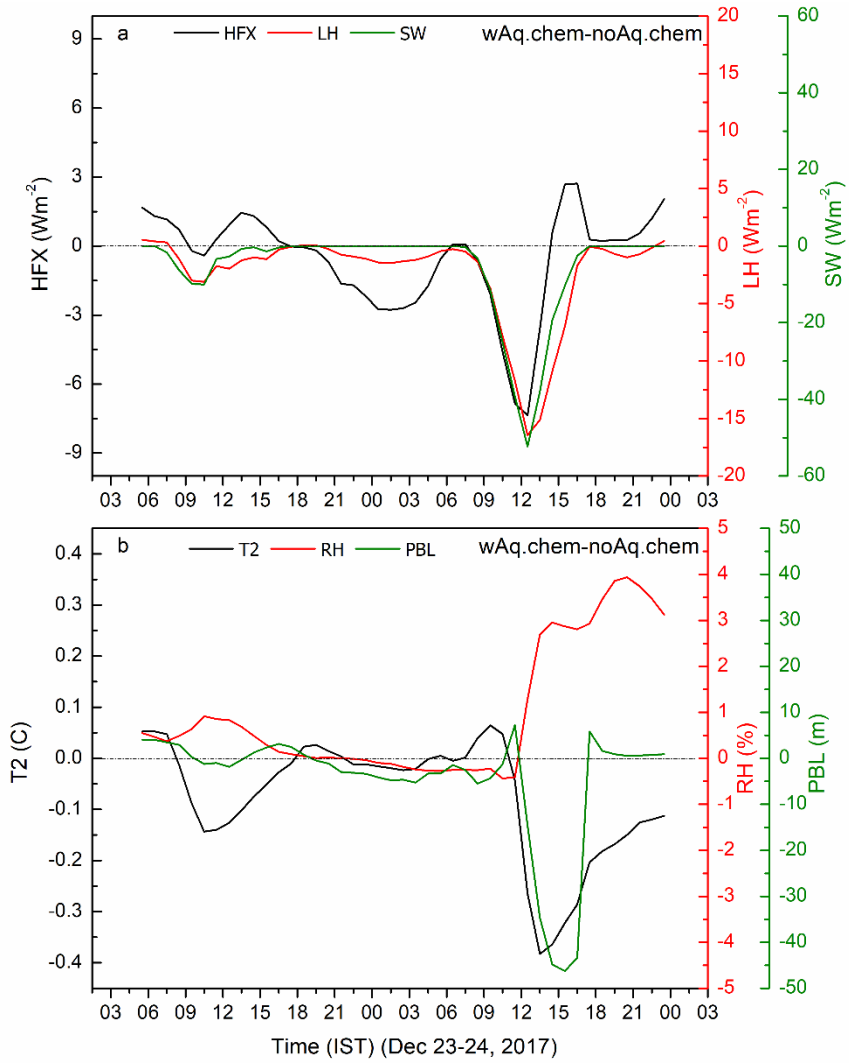
1363

1364

1365 Figure 14 Time series of (a) ΔHFX (sensible heat flux), ΔLH (latent heat flux), and ΔSWF

1366 (downward shortwave flux); (b) ΔT2, ΔRH, and ΔPBL over CIGP (79E-83E,26N-28N), for

1367 23 and 24 December, 2017. Δ denotes the difference between with and without aqueous phase

1368 chemistry.

1369

1370
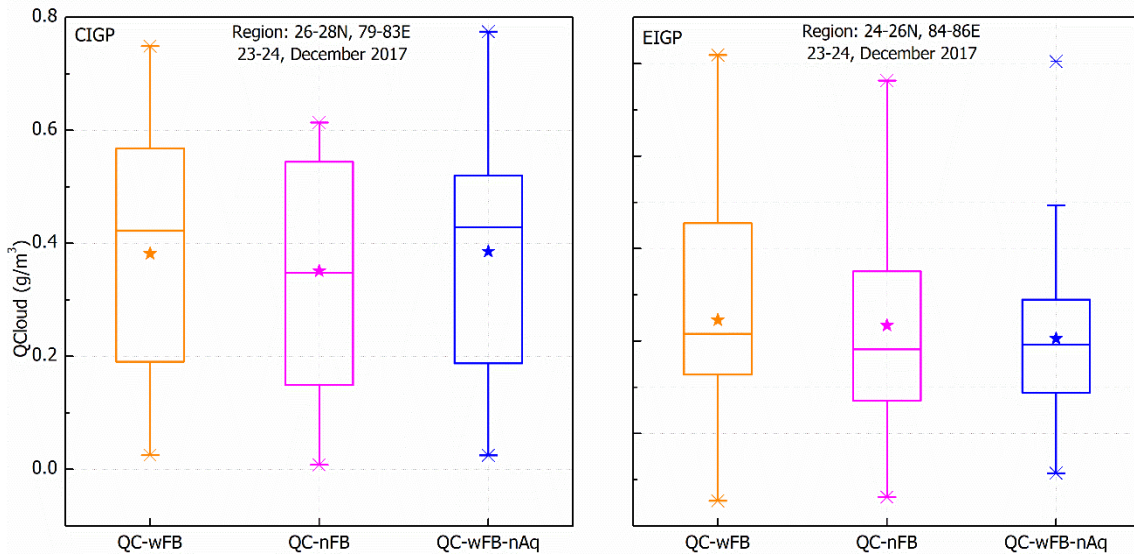
1371
1372

1373 Figure 15 Averages (stars), medians (horizontal lines), quartiles (boxes), maxima, and minima for

1374 LWC (QCloud) averaged over CIGP (left panel) and EIGP (right panel) for the fog event on 23-24

1375 December 2017. Gold is for the simulation with AR feedback and aqueous chemistry, magenta for the

1376 simulation with no AR feedback but includes aqueous chemistry, and blue for the simulation with AR

1377 feedback but no aqueous chemistry. WRF-Chem does not produce fog in the NWIGP during the study

1378 period.

1379

1380

1381

1382

1383

1384

1385

1386

1387

1388

1389

1390

1391

1392

1393

1394

Table 2: Table showing the start and end time of fog1 on 23-24 December 2017 with LWC for the sensitivity experiments, with AR feedback, no AR feedback and no Aqueous phase chemistry

Fog 1 (December 23-24, 2017)

	EXP-wFB			EXP-nFB			EXP-nAq.Chem		
	Start time (IST)	End time (IST)	Duration of Fog	Start time (IST)	End time (IST)	Duration of Fog	Start time (IST)	End time (IST)	Duration of Fog
CIGP	16:30	15:30	**23h**	18:30	17:30	**23h**	18:30	15:30	**21h**
LWC (g m^{-3})	0.034	0.036±0.032		0.141±0.154	0.068±0.005		0.184±0.138	0.034 ±0.021	
Kanpur	05:30	13:30	**8h**	05:30	12:30	**7h**	05:30	12:30	**7h**
LWC (g m^{-3})	0.334± 0.487	0.017		0.458±0.357	0.173± 0.071		0.533	0.025± 0.0123	
Lucknow	23:30	14:30	**15h**	00:30	14:30	**14h**	23:30	14:30	**15h**
LWC (g m^{-3})	0.269±0.145	0.087±0.040		0.232±0.132	0.029±0.024		0.139±0.084	0.025±0.012	
EIGP	21:30	12:30	**15h**	23:30	10:30	**11h**	21:30	10:30	**13h**
LWC (g m^{-3})	0.099±0.092	0.007		0.198±0.188	0.084±0.060		0.026±0.008	0.153±0.119	
Patna	00:30	12:30	**12h**	04:30	10:30	**6h**	02:30	10:30	**8h**
LWC (g m^{-3})	0.100±0.090	0.007		0.009±0.005	0.038±0.041		0.196±0.198	0.166±0.130	
Muzzafarpur	05:30	11:30	**6h**	06:30	10:30	**4h**	06:30	09:30	**3h**
LWC (g m^{-3})	0.112±0.146	0.043±0.057		0.051±0.041	0.003		0.142±0.151	0.157±0.064	

1396 Table 3: Table showing the start time of fog 2 on 24 December 2017 with LWC for the sensitivity

1397 experiments, with AR feedback, no AR feedback and no Aqueous phase chemistry. Fog2 end time

1398 could not be noted as simulation ended on 25 December 2017, 00UT (5:30 IST) before fog2

1399 dissipates.

Fog 2 (December 24, 2017) Start time (IST)		
EXP-wFB	**EXP-nFB**	**EXP-nAq.Chem**
CIGP 19:30	**20:30**	**21:30**
LWC (g m⁻³) 0.025	0.008±0.007	0.025
Kanpur 21:30	22:30	23:30
LWC (g m⁻³) 0.041±0.007	0.298±0.218	0.482±0.398
Lucknow 21:30	20:30	00:30
LWC (g m⁻³) 0.203±0.165	0.005	0.229±0.209
EIGP 00:30	**01:30**	**01:30**
LWC (g m⁻³) 0.024±0.030	0.072±0.088	0.014±0.009
Patna 03:30	03:30	03:30
LWC (g m⁻³) 0.030± 0.046	0.018	0.060
Muzzafarpur 04:30	No fog	No fog
LWC (g m⁻³) 0.159±0.038		

1400

1401

1402